Role of periostin in inflammatory sinonasal disease

Kim, Soo-In

Department of Medical Science

Graduate School

Yonsei University

Role of periostin in inflammatory sinonasal disease

Advisor Kim, Chang-Hoon

A Dissertation Submitted
to the Department of Medical Science
and the Committee on Graduate School
of Yonsei University in Partial Fulfillment of the
Requirements for the Degree of
Doctor of Philosophy in Medical Science

Kim, Soo-In

June 2025

Role of periostin in inflammatory sinonasal disease

**This certifies that the Dissertation
of Kim, Soo-In is approved.**

Thesis Supervisor	Kim, Chang-Hoon
Thesis Committee Member	Cho, Hyung-Ju
Thesis Committee Member	Lee, Sang-Nam
Thesis Committee Member	Shin, Sung-Jae
Thesis Committee Member	Ryu, Ji-Hwan

**Department of Medical Science
Graduate School
Yonsei University**
June 2025

ACKNOWLEDGEMENTS

I would like to express my sincere gratitude to my advisor, Prof. Chang-Hoon Kim, for his continued guidance and support throughout my doctoral studies. His insight and advice has been invaluable to both my research and academic development. I am sincerely grateful to Prof. Hyung-Ju Jo for his academic support and helpful suggestions throughout this study. I also thank Prof. Sang-Nam Lee for her dedication and encouragement, which greatly enriched my doctoral training.

I appreciate my former colleagues, Ji-Suk Ahn and Su-Jin Kim, for their helpful advice and technical guidance. I also thank Bo-ra Kim for her reliable assistance and collaboration. I am grateful to my labmates, Jinsun Kim, SoHyeon An, Miran Kang, Juhee Seo, Yosep Kim, Gyeongyeob Kim, Sol Lee, Min-Seok Koo, and Sungmin Moon for their support and friendship.

Above all, I express my heartfelt appreciation to my beloved family. I am eternally grateful for their unwavering love and encouragement. Without their support, this journey would not have been possible.

Part of this dissertation has been published in a peer-reviewed journal: Kim SI, et al. "*Inflammation-Driven Periostin in ECRS has Contrasting Effects on Tissue Structural Integrity and Osteitis*." *Frontiers in Immunology*. 2025; doi:10.3389/fimmu.2025.1596746.

TABLE OF CONTENTS

LIST OF FIGURES iii

ABSTRACT IN ENGLISH iv

1. INTRODUCTION 1

2. MATERIALS AND METHODS 3

2.1. Cell culture 3

2.1.1. Human nasal epithelial cell culture 3

2.1.2. Human nasal fibroblast culture 4

2.1.3. Human nasal cell co-culture 4

2.1.4. MG63 cell culture 5

2.1.5. Conditioned medium 5

2.2. ECRS mouse model 6

2.2.1 Animals 6

2.2.2. ECRS mouse model 6

2.3. Human ethmoid mucosa 6

2.4. Western blot 7

2.4.1 Cell lysate preperation 7

2.4.2 Western blot 7

2.5. quantitative PCR 8

2.6. ELISA 9

2.7. Histopathology 10

2.8. Immunostaining 10

2.8.1. Immunohistochemistry (IHC) 10

2.8.2. Immunofluorescence (IF) 11
2.9. ALP staining 12
2.10. Statistical analysis 12
3. RESULTS 13
3.1. Expression of periostin in nasal mucosa of CRS patients 13
3.2. Periostin expression in HNEC and HNF by Th2 cytokines 15
3.3. Periostin increased by co-culture of HNEC and HNF 19
3.4. Secreted periostin from nasal fibroblasts mediates osteogenesis of MG63 23
3.5. Effect of periostin deficiency in the ECRS mouse model 25
3.5.1. Expression of periostin in nasal mucosa of the ECRS mouse model 25
3.5.2. Effects of periostin deficiency on inflammation in the ECRS mouse model 28
3.5.3. Effects of periostin deficiency on osteitic changes in the ECRS mouse model 32
3.5.4. Effects of periostin deficiency on tissue remodeling in the ECRS mouse model 35
4. DISCUSSION 40
5. CONCLUSION 45
REFERENCES 46
ABSTRACT IN KOREAN 51

LIST OF FIGURES

<Fig 1> Periostin expression in nasal mucosa and osteitis score of non-ECRS and ECRS patients 14
<Fig 2> Periostin expression in human nasal cells by cytokines 17
<Fig 3> Level of periostin from co-culture of HNEC and HNF with IL-4 21
<Fig 4> Secreted periostin from nasal fibroblasts by IL-4 mediated osteogenesis of MG63 24
<Fig 5> Protocols for the development of eosinophilic rhinosinusitis in WT and periostin knock-out mice 26
<Fig 6> Periostin expression in the nasal mucosa of WT and periostin KO mice in the ECRS model. 27
<Fig 7> Effect of periostin deficiency on eosinophil infiltration in the ECRS mouse model 30
<Fig 8> Effect of periostin deficiency on goblet cell hyperplasia in the ECRS mouse model 31
<Fig 9> Effect of periostin deficiency on osteogenesis in the ECRS mouse model 33
<Fig 10> Effect of periostin deficiency on tissue remodeling in the ECRS mouse model 37
<Fig 11> The two faces of periostin in ECRS 44

ABSTRACT

Role of periostin in inflammatory sinonasal diseases

Periostin, a matricellular protein, is recognized as a biomarker of type 2 inflammation in chronic respiratory diseases, including asthma and chronic rhinosinusitis (CRS), and is involved in airway remodeling. While CRS is often linked to an increased level of periostin in tissue and serum, its role in the pathology of CRS remains unclear.

This study aims to identify the main source of periostin in the sinonasal mucosa and to investigate its role in either exacerbating chronic inflammation or protecting the nasal epithelium from tissue remodeling in inflammatory sinonasal diseases. In addition, we aimed to examine the association between secreted periostin, Th2 inflammation, and osteogenesis in eosinophilic CRS (ECRS).

As a result, primary human nasal epithelial cells (HNECs) and fibroblasts (HNFs) were derived from nasal polyps. Interleukin-4 increased periostin expression in both the lysates and media of these cells. Periostin was secreted more by HNFs than by HNECs, indicating that HNFs are the main source of IL-4-induced periostin. Additionally, periostin secreted by HNFs induced osteoblast differentiation. In the ECRS mouse model using periostin knockout (KO) mice, the wild-type group showed increased periostin levels, thicker epithelium, and greater nasal bone thickness. The KO group exhibited significantly lower RUNX2 and osteopontin expression. However, eosinophil infiltration and goblet cell metaplasia did not differ significantly between groups.

In summary, periostin is mainly secreted from nasal fibroblasts in response to Th2 cytokines, and the secreted periostin maintains ECM structure and mediates osteogenesis in sinonasal bone. In conclusion, in chronic sinusitis, periostin has the dual effect of protecting tissue structure and promoting osteogenic remodeling.

Key words : periostin, sinonasal mucosa, osteitis, chronic rhinosinusitis

1. Introduction

Periostin (also known as Osteoblast-Specific Factor 2), a member of the matricellular protein family, has been identified as a key contributor in various biological processes such as tissue remodeling, metastasis, and cancer.[1-3]. Periostin contributes to fibrosis, epithelial-mesenchymal transition, and Th2-driven inflammation, processes relevant to diseases such as cancer, asthma, and idiopathic pulmonary fibrosis[4-6]. The expression of periostin is regulated by cytokines including interleukin-4 (IL-4), interleukin-13 (IL-13), interleukin-5 (IL-5) and bone morphogenetic protein 2 (BMP-2)[7-11].

Recent studies have shown that periostin undergoes extensive alternative splicing, particularly at its C-terminal domain, which may influence its diverse biological functions such as tissue regeneration, angiogenesis, and immune modulation[12-14]. These splice variants are regulated by upstream signals such as neuregulin and TGF-β, which can alter periostin's localization and its interactions with extracellular components[15,16]. At least eleven isoforms have been identified across different tissues and developmental stages[17-20].

Research has demonstrated that fibroblasts release periostin to control the deposition of collagen, which in turn modifies the mechanical properties of connective tissues[21]. Periostin interacts with extracellular matrix (ECM) components such as tenascin and fibronectin, and with integrins like αvβ3 and αvβ5[22]. Its interaction with integrins such as αvβ3 and αvβ5 stimulates FAK/PI3K/AKT signaling pathways that promote inflammation, extracellular matrix production, and changes in cell phenotype[23]. In allergic and fibrotic diseases, periostin influences multiple signaling cascades including NF-κB, PI3K/AKT, and FAK pathways via interaction with integrins such as αvβ3 and αvβ5, thereby regulating downstream genes like α-SMA, TGF-β1, and chemokines including Ccl2 and Cxcl1[24-27]. Through these mechanisms, periostin serves as a nodal point linking inflammation, matrix remodeling, and immune cell recruitment. Its ability to bind heparin and heparan sulfate proteoglycans further expands its ECM interactions[13].

In addition, periostin interacts with the TGF-β signaling system to enhance profibrotic responses and ECM remodeling, thereby advancing the development of fibrosis in chronic inflammatory conditions[8]. Periostin also facilitates the recruitment and infiltration of eosinophils, contributing to inflammatory disorders such as bronchial asthma and eosinophilic chronic rhinosinusitis (ECRS)[28,29].

Chronic rhinosinusitis (CRS) is an inflammatory sinonasal disease characterized by inflammation of the nose and paranasal sinuses lasting at least 12 weeks[30]. Eosinophilic chronic rhinosinusitis (ECRS), a subtype of CRS, is associated with severe eosinophilic infiltration and nasal polyps. ECRS is caused by Th2 immune responses which stimulates IgE production and eosinophil infiltration[31]. Elevated levels of periostin have been consistently detected in the sinonasal mucosa of patients with CRS, particularly in those with eosinophilic inflammation and nasal polyps[32].

Moreover, increased periostin concentrations in blood and tissue are closely correlated with both circulating and tissue-infiltrating eosinophil levels, underscoring periostin's role in modulating eosinophilic activity[33-35]. Periostin further enhances local tissue eosinophilia by supporting eosinophil adhesion and migration through αMβ3 integrin-mediated mechanisms, which is particularly relevant in allergic diseases such as asthma and ECRS[36].

Periostin contributes to remodeling of the mucosal tissue by interacting with extracellular matrix components such as fibronectin and tenascin-C, thereby facilitating collagen synthesis and subepithelial fibrosis[37]. Fibronectin, a key ECM glycoprotein, provides a scaffold for collagen fibrillogenesis and cell adhesion[21]. Although inflammation is involved in these processes, the exact relationship between inflammation and remodeling remains unclear and requires additional research to properly comprehend the underlying mechanisms.

Cases of CRS patients often show thickening of the bones in the paranasal sinuses, which is referred to as osteitis or osteoneogenesis. These osteitic changes are associated with endoscopic and radiologic severity scores, including CT, endoscopy, and olfactory scores[38]. Osteitis scores measured by CT are also associated with tissue and serum eosinophilia in CRS patients[39,40]. Elevated periostin expression, together with eosinophil infiltration, may contribute to these osteitic alterations in chronic rhinosinusitis, suggesting that periostin plays a role in inflammation-induced bone remodeling.

This study aims to identify the cellular sources of periostin in the sinonasal mucosa under inflammatory conditions and to elucidate the role of inflammation-induced periostin in modulating the pathophysiological mechanisms underlying ECRS. Furthermore, it seeks to determine whether periostin contributes to the exacerbation of chronic inflammation or, alternatively, plays a protective role by preserving epithelial integrity in inflammatory sinonasal conditions.

2. MATERIALS AND METHODS

2.1. Cell culture

2.1.1. Human nasal epithelial cell culture

Human nasal tissues were obtained during surgery from nasal polyps of patients with chronic rhinosinusitis (CRS). This procedure was approved by the Ethics Committee of Yonsei University College of Medicine. Tissues were treated overnight at 4 °C with 0.1% type XIV protease (Sigma-Aldrich, USA) in Dulbecco's Modified Eagle Medium and Ham's F-12 nutrient mixture (DMEM/F12) supplemented with penicillin G sodium (50 IU/mL) and streptomycin sulfate (50 μg/mL). Dissociated epithelial cells were washed three times in DMEM/F12 containing antibiotics and resuspended in DMEM/F12 supplemented with antibiotics and 10% fetal bovine serum (FBS; Gibco, USA). Cells were pre-plated on plastic dishes at 37 °C for 1 hour to allow differential attachment and removal of fibroblasts. Suspended epithelial cells were then seeded at 3×10^4 cells per dish (500 cells/cm²) into 10-cm plastic tissue culture dishes. The culture medium used was Bronchial Epithelial Cell Growth Medium BulletKit (BEGM; Lonza, Switzerland) containing hydrocortisone 21-hemisuccinate (0.5 μg/mL), insulin (5 μg/mL), transferrin (10 μg/mL), epinephrine hydrochloride (0.5 μg/mL), 3,3´,5-triiodo-L-thyronine (6.5 ng/mL), gentamicin sulfate (50 μg/mL), and amphotericin B (50 μg/mL), all supplied by Clonetics, USA. The medium was further supplemented with epidermal growth factor (EGF; 25 ng/mL; Collaborative Research, USA), all-trans retinoic acid (1×10^{-7} mol/L; Sigma-Aldrich, USA), bovine serum albumin (1.5 mg/mL; Sigma-Aldrich), and bovine pituitary extract (1% v/v; Pel-Freez Biologicals, USA). Cultures were maintained at 37 °C in a humidified 5% CO_2 atmosphere. The culture medium was replaced on day 1 after seeding and subsequently changed every other day until cultures reached 50–60% confluency. At this stage, cells were dissociated using trypsin-EDTA (Clonetics, USA) and counted using a hemocytometer. They were then subcultured as described above for further passages. Cells not used for reestablishing cultures were either suspended in BEGM supplemented with 10% dimethyl sulfoxide at a concentration of $1–2 \times 10^6$ cells/mL and cryopreserved in liquid nitrogen, or tested for their differentiation competence. Serially passaged NHNE cells (1×10^5 cells per culture; 2×10^4 cells/cm²) were seeded in 0.5 mL of culture medium into 12-mm Transwell-clear culture

inserts with 0.4-μm pore size (Costar, USA). Cells were cultured in a 1:1 mixture of BEGM and DMEM containing all supplements as previously described, except that EGF was reduced to 0.5 ng/mL. The cultures were maintained submerged for the first 2–3 days, with media changed on day 1 and then every other day. The air–liquid interface (ALI) was established by removing the apical medium and feeding solely from the basal compartment. ALI culture medium was replaced every 2 days, with retinoic acid (50 nM) added. Additional cytokines (IL-4, IL-13, IL-1β, TNF-α, and IFN-γ; 5 ng/mL each) were added to the basal compartment as required.

2.1.2. Human nasal fibroblast culture

After removing nasal epithelial cells from the nasal polyp tissue, the remaining tissue was washed twice with PBS. The nasal polyp was then minced into small pieces using scissors in a 10-cm culture dish. Ten milliliters of fibroblast culture medium was added, consisting of RPMI 1640 (Lonza, Switzerland), 10% fetal bovine serum (FBS; Gibco, USA), sodium pyruvate (100 mM; Gibco, USA), L-glutamine (200 mM; Gibco, USA), MEM Non-Essential Amino Acids Solution (100×; Gibco, USA), and penicillin-streptomycin (5000 U/mL; Gibco, USA). Cells were subcultured before reaching 80% confluency, and experimental treatments were performed at passage 2, using cells seeded into 12-well plates. Before treatment, the cells were starved overnight in fibroblast serum-free medium containing RPMI 1640 (Lonza, Switzerland), bovine serum albumin (BSA; 1 mg/mL; Gibco, USA), sodium pyruvate (100 mM; Gibco, USA), L-glutamine (200 mM; Gibco, USA), MEM Non-Essential Amino Acids Solution (100×; Gibco, USA), and penicillin-streptomycin (5000 U/mL; Gibco, USA). During early culture establishment, immunocytochemistry for vimentin was performed to confirm fibroblast identity, and α-smooth muscle actin (α-SMA) staining was used to assess fibroblast activation and determine appropriate passage ranges for experiments. Cytokines (IL-4, IL-13, IL-1β, TNF-α, and IFN-γ; 5 ng/mL each) were added directly to the culture medium covering the HNFs in accordance with experimental protocols.

2.1.3. Human nasal cell co-culture

For the epithelial–fibroblast co-culture model, human nasal epithelial cells (HNECs) were cultured on Transwell inserts at an air–liquid interface (ALI) for 14 days to promote cellular differentiation and maturation. Concurrently, human nasal fibroblasts (HNFs) were seeded onto the basolateral surface of a 12-well tissue culture plate, matching the dimensions of the Transwell plate.

The seeding density for the HNFs was 1×10^4 cells per well. Following seeding, HNFs were serum-starved overnight to synchronize their metabolic activity. After the starvation period, the Transwell inserts containing ALI-day 14 HNECs were transferred into the 12-well plate, suspended above the wells containing HNFs. To stimulate both cell types during co-culture, IL-4 (5 ng/mL) was added to the basal compartment beneath the Transwell inserts.

2.1.4. MG63 cell culture

MG63 (ATCC, USA) is a fibroblast-like osteosarcoma cell line derived from human bone. MG63 cells were subcultured in 75 cm^2 flasks using culture medium consisting of Earle's Balanced Salt Solution (EBSS; Gibco, USA), 2 mM L-glutamine (Gibco, USA), 10% fetal bovine serum (FBS; Gibco, USA), and 100× non-essential amino acids (NEAA; Gibco, USA). For starvation, the culture medium was replaced overnight with fibroblast serum-free medium containing EBSS (Gibco, USA), 2 mM L-glutamine (Gibco, USA), and 100× NEAA (Gibco, USA). Following starvation, cells were cultured in osteogenic differentiation medium consisting of fibroblast serum-free medium supplemented with ascorbic acid (50 μg/mL; Sigma-Aldrich, USA) and β-glycerophosphate (10 mmol/L; Sigma-Aldrich, USA).

2.1.5. Conditioned medium

Human nasal fibroblasts (HNFs) were treated with interleukin-4 (IL-4; 5 ng/mL) for 2 days, after which the culture supernatant was collected. To selectively retain periostin while removing IL-4 and other low-molecular-weight cytokines, the conditioned medium was concentrated using Amicon Ultra centrifugal filter units (30 kDa molecular weight cutoff; Millipore, USA). This filtration step effectively excluded IL-4 (~15–20 kDa) while retaining secreted periostin. The resulting concentrated medium was referred to as Secretion(HNF), and was used in subsequent experiments. Periostin concentration in Secretion(HNF) was quantified using an enzyme-linked immunosorbent assay (ELISA; R&D Systems, USA; DY3548B). To normalize periostin levels across conditions, recombinant human periostin (rhPOSTN) was diluted to 200 ng/mL, and Secretion(HNF) was adjusted to the same concentration based on ELISA results. To inhibit periostin function in Secretion(HNF), the medium was pretreated with a periostin-neutralizing antibody (R&D Systems, USA; AF3548) at a final concentration of 10 μg/mL, corresponding to the neutralization of

200 ng/mL periostin. The antibody was added directly to Secretion(HNF) and incubated for 1 hour at 37 °C prior to application to cells.

2.2. ECRS model

2.2.1. Animals

C57BL/6J female mice (6 weeks old) were purchased from Jackson Laboratory (USA) and maintained under specific pathogen-free (SPF) conditions. Periostin knockout (KO) mice were kindly provided by Prof. Sang-Wook Kim (Gyeongsang National University Hospital, Republic of Korea). All animal procedures were approved by the Institutional Animal Care and Use Committee (IACUC) of Yonsei University Health System (approval number: 2024-0048), and the study was conducted in compliance with international guidelines, including the ARRIVE (Animal Research: Reporting of In Vivo Experiments) standards.

2.2.2. ECRS mouse model

Mice were intranasally administered a mixture of airborne allergens three times per week for 12 weeks in the wild-type (WT) ECRS and periostin knockout (KO) ECRS groups. Phosphate-buffered saline (PBS)-treated mice served as controls for both WT and KO groups (i.e., WT PBS and periostin KO PBS groups, respectively). The allergen mixture included 20 μg of house dust mite (HDM) extract (*Dermatophagoides pteronyssinus*; Greer Laboratories, Lenoir, NC, USA), 20 μg of *Aspergillus fumigatus* (Greer Laboratories), 20 μg of *Alternaria alternata* (Greer Laboratories), and 1 μg of *S. aureus*–derived protease (Abnova, Taipei, Taiwan), dissolved in sterile PBS to a total volume of 30 μL. Each mouse received 15 μL per nostril via intranasal instillation. Mice were sacrificed and analyzed at week 12, following procedures adapted from a previously published study[41]. Although blinding during treatment and outcome assessment was not feasible due to experimental constraints, all tissue processing, sampling locations, and data analysis procedures were standardized and applied uniformly across all groups to minimize potential bias.

2.3. Human ethmoid mucosa

Human nasal ethmoid mucosa samples were obtained during surgery from 23 patients diagnosed with septal deviation or maxillary cancer. The specimens used in this study were collected from anatomically normal regions adjacent to the tumor. This procedure was approved by the Ethics

Committee of Yonsei University College of Medicine. To facilitate different preparation methods for subsequent analyses, each tissue sample was divided into two equal halves. One half was fixed in 4% paraformaldehyde overnight, followed by paraffin embedding to generate formalin-fixed paraffin-embedded (FFPE) blocks. The other half underwent protein extraction. Frozen tissue was pulverized in the presence of liquid nitrogen using a mortar and pestle. After the nitrogen had evaporated, radioimmunoprecipitation assay (RIPA) buffer supplemented with a protease inhibitor cocktail was added to the finely ground tissue. The sample was incubated on ice for over 1 hour and then centrifuged at 12,000 rpm for 15 minutes at 4 °C. The resulting supernatant (lysate) was transferred to a fresh tube for subsequent analysis. This study was reviewed and approved by the Institutional Review Board of Severance Hospital (IRB No. 4-2021-0573) and conducted in accordance with the ethical standards outlined in the Declaration of Helsinki.

2.4. Western blot

2.4.1. Cell lysate preperation

Cell culture dishes were washed thoroughly with phosphate-buffered saline (PBS). Following washing, PBS was completely aspirated, and ice-cold lysis buffer (RIPA buffer supplemented with a protease inhibitor cocktail) was added. Adherent cells were gently scraped using a cell scraper to detach and collect all cells. The cell suspension was transferred into a pre-chilled microcentrifuge tube (1.5 mL Eppendorf tube) and placed on ice for 40 minutes to preserve protein integrity. After incubation, the lysates were centrifuged at 12,000 rpm for 15 minutes at 4 °C to pellet cellular debris and insoluble materials. The clear supernatant was carefully transferred to a fresh pre-chilled tube and stored on ice until further analysis.

2.4.2. Western blot

Protein concentrations of the cell lysates were determined using a bicinchoninic acid (BCA) assay. Lysates were diluted to a final concentration of 20 μg per lane, and mixed 1:1 (v/v) with 5× SDS sample buffer. Samples were boiled at 95 °C for 5 minutes and immediately cooled on ice. Proteins were separated by electrophoresis using 8% or 12% SDS–polyacrylamide gels (SDS-PAGE), with equal protein amounts loaded per lane. A pre-stained molecular weight marker was included in one lane. The gels were run in 1× running buffer at 80 V until optimal separation was achieved. Polyvinylidene difluoride (PVDF) membranes were activated in 100% methanol for 20 seconds,

rinsed with distilled water for 2 minutes, and equilibrated in 1× transfer buffer for 5 minutes. A transfer sandwich was assembled (sponge–filter paper–gel–membrane–filter paper–sponge) and placed into a transfer cassette. Protein transfer was performed for 2 hours at a constant current of 210 mA. Following transfer, membranes were briefly washed with 1× TBST (Tris-buffered saline with Tween 20) and then blocked with 5% (w/v) skim milk or bovine serum albumin (BSA) in 1× TBST for 1 hour at room temperature with gentle rocking. Primary antibodies were diluted to working concentrations in blocking solution and incubated with the membrane overnight at 4 °C with gentle rocking. Membranes were then washed three times for 10 minutes each with 1× TBST. After washing, membranes were incubated with the appropriate HRP-conjugated secondary antibody diluted in 1× TBST (containing 5% milk or BSA) for 1 hour at room temperature with gentle agitation. Membranes were subsequently washed three times with 1× TBST and twice with 1× TBS, each for 5 minutes, under gentle rocking conditions. Enhanced chemiluminescence (ECL) reagent was added to the membrane and incubated for 1 minute. The membrane was then placed between transparency films (OHP) and air bubbles were carefully removed. Finally, the membrane was exposed to autoradiography film in a darkroom and developed accordingly.

2.5. quantitative PCR

Total RNA was extracted using TRIzol Reagent (Invitrogen, Gaithersburg, MD, USA) according to the manufacturer's protocol. To eliminate genomic DNA contamination, samples were treated with RNase-free DNase I (New England Biolabs, Ipswich, MA, USA) prior to reverse transcription. 1 μg of total RNA was reverse transcribed using M-MLV Reverse Transcriptase (Thermo Fisher Scientific, Carlsbad, CA, USA). For quality validation, direct sequencing of the resulting cDNA was performed using the 3730xl DNA Analyzer (Applied Biosystems, Foster City, CA, USA). Quantitative real-time PCR (qRT-PCR) was carried out using a 7300 Real-Time PCR System (Applied Biosystems, Foster City, CA, USA) and the KAPA SYBR® FAST qPCR Kit (Roche, Indianapolis, IN, USA) in accordance with the manufacturer's instructions. The primers used for the qPCR reactions: POSTN (Mouse)-F (5'-CAG CAA ACC AC T TTC ACC GAC C-3') and POSTN (Mouse)-R (5'-AGA AGG CGT TGG TCC ATG CTC A-3') for the mouse periostin gene, POSTN (Human)-F (5'- GCT ATT CTG ACG CCT CAA AAC T -3') and POSTN (Human)-R (5'- AGC CTC ATT ACT CGG TGC AAA -3') for the mouse periostin gene, ALP (Human)-F (5'-TTG GGC AGG CAA GAC ACA-3') and ALP (Human)-R (5'-GAA GGG AAG GGA TGG AGG AG-3') for

the human alkaline phosphatase gene, and OCN (Human)-F (5'-ACC ATC TTT CTG CTC ACT CTG CT-3') and OCN (Human)-R (5'-CCT TAT TGC CCT CCT GCT TG-3') for the human osteocalcin gene.

2.6. ELISA

Periostin concentrations were measured using the Human Periostin/OSF-2 DuoSet ELISA kit (R&D Systems, Minneapolis, MN, USA) according to the manufacturer's protocol. To prepare the assay plate, the capture antibody was diluted to the working concentration in PBS without carrier protein and 100 μL per well was added to a 96-well microplate. The plate was sealed and incubated overnight at room temperature. Each well was then aspirated and washed three times with 400 μL of Wash Buffer using a squirt bottle, manifold dispenser, or automated washer. Complete removal of liquid at each step was ensured by aspirating or inverting the plate onto clean absorbent paper. Following washing, 300 μL of Reagent Diluent was added to each well to block nonspecific binding. The plate was incubated at room temperature for at least 1 hour. After blocking, the aspiration/wash step was repeated as described above. Then, 100 μL of either sample or standard diluted in Reagent Diluent (or other appropriate diluent) was added to each well. The plate was covered with an adhesive strip and incubated for 2 hours at room temperature. After incubation, the plate was washed three times as described. Next, 100 μL of Detection Antibody diluted in Reagent Diluent was added per well, sealed, and incubated for another 2 hours at room temperature. Following three additional washes, 100 μL of a working dilution of streptavidin-HRP was added to each well, and the plate was incubated for 20 minutes at room temperature, avoiding direct light exposure. After a final wash cycle, 100 μL of Substrate Solution was added to each well and incubated for 20 minutes at room temperature in the dark. Then, 50 μL of Stop Solution was added to each well, and the plate was gently tapped to mix. Absorbance at 450 nm was immediately measured using a microplate reader. For ELISA analysis of tissue and culture samples, human tissue samples were homogenized in RIPA buffer supplemented with protease inhibitors and lysed on ice. Protein concentration was measured using the BCA assay (Thermo Fisher Scientific, Waltham, MA, USA) to ensure equal protein loading across samples. Conditioned media from cell culture experiments were collected directly without further processing. For Transwell-based cultures of HNECs, the apical and basal compartments were collected separately. For apical sampling, 200 μL of PBS was gently applied to the apical surface, then carefully aspirated using light pipetting to avoid disturbing the epithelium. Basal media from

both HNECs and co-cultured HNFs were harvested directly from the bottom compartment. Equal total protein concentrations were applied across all measured conditions to allow accurate comparison of periostin levels.

2.7. Histopathology

The mouse heads were fixed in 4% paraformaldehyde (PFA) overnight, decalcified in 10% ethylenediaminetetraacetic acid (EDTA) for 2 weeks, and embedded in paraffin. The embedded tissues were then sectioned coronally into 4-μm-thick slices. To standardize the anatomical locations examined and ensure reproducibility across samples, an atlas of normal murine sinonasal anatomy was referenced. Histological changes in the nasal mucosa were analyzed by using the following staining methods: hematoxylin and eosin (H&E) staining for overall inflammation; Sirius Red staining for eosinophil infiltration and polyp-like lesions; periodic acid–Schiff (PAS) staining for goblet cell hyperplasia; and Masson's Trichrome staining for collagen deposition and assessment of epithelial and subepithelial thickness. The anatomical sites of measurement were standardized for each mouse. Tissue eosinophil aggregates were defined as one or more clusters of eosinophils (>20 per high-power field) within the sinonasal mucosa. The numbers of eosinophils and goblet cells were counted in nine high-power fields (×400) per mouse and summed for comparison between groups. The maximum mucosal thickness at the transition zone between the olfactory and respiratory epithelium was measured, and the average from four different regions was used for quantitative comparison. Collagen deposition was quantified in each section and expressed as the percentage of collagen-stained area relative to the total subepithelial area, using ImageJ software (version 1.51j8; National Institutes of Health, USA).

2.8. Immunostaining

2.8.1. Immunohistochemistry (IHC)

Formalin-fixed paraffin-embedded (FFPE) sections (4 μm thick) were dewaxed in xylene (Sigma-Aldrich, St. Louis, MO, USA), rehydrated through a graded ethanol series, and subjected to antigen retrieval by microwave heating in 0.01 mol/L sodium citrate buffer (pH 6.0). Endogenous peroxidase activity was quenched by incubation with 3% methanolic hydrogen peroxide for 10 minutes at room temperature. Non-specific binding was blocked by incubating the tissue sections with 10% normal serum from the VECTASTAIN Elite ABC Kit (Vector Laboratories, Burlingame, CA, USA) for 30

minutes at room temperature. Primary antibodies were applied at 4 °C overnight (24 h), with the following dilutions: anti-RUNX2 (ab192286, Abcam, UK; 1:200) and anti-periostin (ab14041, Abcam, UK; 1:250). Following rinsing with TBS, the sections were incubated for 30 minutes at room temperature with a horseradish peroxidase (HRP)-conjugated, species-specific secondary antibody (Vector Laboratories, 1:5000 dilution). The signal was amplified using the indirect immunoperoxidase method with the DAKO EnVision+ System (Dako, Kingsgrove, Australia). Tissue sections were counterstained with Gill's hematoxylin (Sigma-Aldrich, St. Louis, MO, USA), dehydrated through ethanol, cleared in xylene, and mounted with DPX mounting medium (ProSciTech, Thuringowa, QLD, Australia).

2.8.2. Immunofluorescence (IF)

Formalin-fixed paraffin-embedded (FFPE) sections, cut at 4 μm thickness, were dewaxed in xylene (Sigma-Aldrich, St. Louis, MO, USA). Following dewaxing, the sections were rehydrated through a graded ethanol series, starting from absolute ethanol (100%) and subsequently through 95%, 80%, and 70% ethanol. Antigen retrieval was performed using microwave heating in 0.01 mol/L sodium citrate buffer (pH 6.0). Sections were treated with 3% methanolic hydrogen peroxide for 10 minutes at room temperature, followed by a 5-minute wash in Tris-buffered saline with Tween 20 (TBST). Non-specific binding was blocked by incubating the sections with 5% bovine serum albumin (BSA; Sigma-Aldrich, USA) for 1 hour at room temperature. Following blocking, the sections were incubated overnight at 4 °C with the appropriate primary antibodies, all diluted 1:200 in DakoCytomation Antibody Diluent (Agilent, Santa Clara, CA, USA). The primary antibodies used were: anti-fibronectin (ab2413, Abcam, UK), anti-periostin (AF2955, R&D Systems, Minneapolis, MN, USA), anti-osteopontin (ab218237, Abcam, UK), and anti-α-SMA (ab5694, Abcam, UK). After incubation, sections were washed three times for 5 minutes each in TBST to remove unbound antibodies. They were then incubated with a fluorophore-conjugated secondary antibody (diluted 1:1000 in DakoCytomation Antibody Diluent) for 1 hour at room temperature. After secondary antibody incubation, the sections were stained with DAPI (4′,6-diamidino-2-phenylindole; diluted 1:1000 in distilled water) for 10 minutes to visualize nuclei. Following final washes, coverslips were mounted using VECTASHIELD Mounting Medium (Vector Laboratories, Burlingame, CA, USA). Slides were analyzed under a confocal laser-scanning microscope (LSM700, Carl Zeiss MicroImaging GmbH, Jena, Germany).

2.9. ALP staining

To assess osteogenic differentiation, alkaline phosphatase (ALP) staining was performed using the Alkaline Phosphatase Staining Kit (ab284936, Abcam, Cambridge, UK) in accordance with the manufacturer's instructions. MG63 cells were seeded into 12-well culture plates (Corning, USA) and maintained under the specified experimental conditions. Following the desired treatment period, the cells were fixed with the fixative solution provided in the kit for 1–2 minutes at room temperature (20–25 °C). After fixation, cells were incubated with the ALP staining solution for 15–30 minutes in the dark. The stained cells were gently rinsed with distilled water and observed under a standard light microscope (Olympus, Japan). The intensity and distribution of ALP-positive staining were analyzed to evaluate the degree of osteogenic activity.

2.10. Statistical analysis

Statistical analyses were performed using GraphPad Prism v.8. All quantitative data are expressed as the mean ± standard error of the mean (SEM). For the in vivo experiments, six mice per group were used. Among them, four mice were allocated for histological analyses, and the remaining two were used for protein and RNA extraction.

3. RESULTS

3.1. Expression of periostin in nasal mucosa of CRS patients

First, nasal mucosal tissues from CRS patients were classified according to the JESREC scoring system, which is based on eosinophil counts in peripheral blood and further confirmed by quantifying tissue eosinophils per high-power field (HPF) following Sirius Red staining (Fig. 1A). Patients with eosinophil counts exceeding 70 cells/HPF were classified as having eosinophilic CRS (ECRS), while the remaining were categorized as non-eosinophilic CRS (non-ECRS). Based on this classification, periostin expression and osteitis severity were evaluated in the ECRS, non-ECRS, and normal control groups.

To evaluate periostin expression in the nasal mucosa, IHC was performed using a periostin-specific antibody, with signals visualized using 3,3´-diaminobenzidine (DAB) chromogenic detection (brown). Periostin was primarily localized in the subepithelial region in all groups, including normal controls; however, expression was markedly elevated in the ECRS group compared to both the non-ECRS and normal groups (Fig. 1A).

For quantitative validation, periostin levels in nasal tissue lysates were measured by ELISA. Both CRS groups exhibited significantly higher periostin concentrations than the normal group, with the ECRS group demonstrating significantly elevated levels compared to the non-ECRS group ($P \leq 0.05$) (Fig. 1B).

To assess bony involvement, osteitis scores were calculated using the Global Osteitis Scoring Scale, which quantifies sinonasal bone thickening on computed tomography (CT) scans. Both CRS groups showed significantly increased osteitis scores relative to the normal group ($P \leq 0.001$), and the ECRS group exhibited significantly higher scores than the non-ECRS group ($P \leq 0.01$) (Fig. 1C).

Finally, correlation analysis revealed a positive association between periostin levels and osteitis scores ($r > 0.3$), suggesting that elevated periostin expression may contribute to the development of osteitis in CRS patients (Fig. 1D).

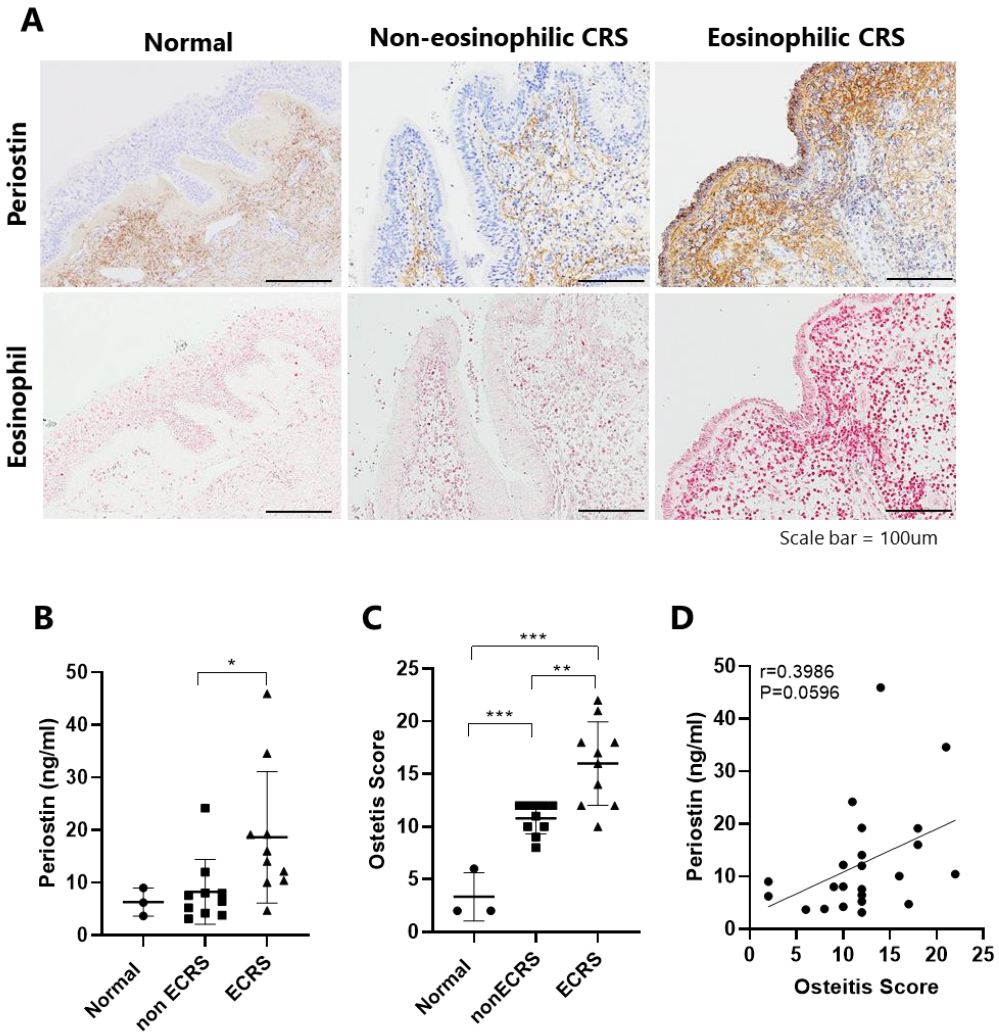

Figure 1. Periostin expression in nasal mucosa and osteitis scroe of non-ECRS and ECRS paitients. Analyse human nasal ethmoid mucosa from CRS paitients. Non-ECRS and ECRS group by JECSREC and number of eosinophils in high per field.(A) Comparison of expression of periostin between non-ECRS and ECRS. b-actin serves as a loading control.(Scale bar = 100um) (B) Comparssion of periostin concentraion in ethmoid mucosa between non-ECRS and ECRS by ELISA. (C) Comparssion of ostetis score between non-ECRS and ECRS evaluated by CT. (D) Correlarion of osteitis scroe and level of periosin in nasal mucosa. (Normal n=3, non-ECRS n=10 and ECRS n=10) *P $\leq$ 0.05, **P $\leq$ 0.01, ***P $\leq$ 0.001.

3.2. Periostin expression in HNEC and HNF by Th2 cytokines

Epithelial cells and fibroblasts derived from human nasal polyps were used to determine whether periostin levels in the sinonasal region are elevated in response to Th2 cytokines, as has been reported in other regions of the airway. In addition, the study evaluated the effects of non-Th2 cytokines on periostin expression.

Human nasal epithelial cells (HNECs) were cultured from basal cells isolated from the apical surface of nasal polyps. These basal cells were seeded onto Transwell membranes with the apical surface exposed to air and the basolateral surface in contact with culture medium. This air–liquid interface (ALI) culture system facilitated the differentiation of nasal epithelial cells by mimicking the native mucosal environment. After 14 days of ALI culture, the HNECs differentiated into a pseudostratified epithelium composed of ciliated cells, goblet cells, and sustentacular cells, resembling the human nasal mucosa. Human nasal fibroblasts (HNFs) were isolated from enzymatically dissociated nasal polyp tissue and cultured under standard conditions. Only early-passage HNFs were used in this study.

Both HNECs and HNFs were treated with various cytokines, including IL-4, IL-13, IL-1β, TNF-α, and IFN-α, at a concentration of 5 ng/mL. Cells were harvested on days 0, 1, and 2 for analysis.

Western blot analysis of cell lysates demonstrated that periostin expression increased in HNECs only in response to IL-4, and this increase was statistically significant on day 1 when compared with the control ($P \leq 0.05$). In contrast, in HNFs, periostin expression was significantly elevated in response to both IL-4 and IL-13 on day 2 ($P \leq 0.01$) (Fig. 2A).

This pattern was corroborated by ELISA of the concentrated culture supernatants, which showed that secreted periostin increased in parallel with intracellular levels. In HNECs, IL-4 stimulation significantly increased periostin secretion on day 1 ($P \leq 0.05$), with an even greater increase observed on day 2 ($P \leq 0.001$) compared to day 0. In HNFs, both IL-4 and IL-13 significantly increased periostin secretion on day 2 ($P \leq 0.001$) (Fig. 2B).

POSTN mRNA expression was also analyzed by quantitative real-time PCR. In HNECs, IL-4 treatment significantly increased POSTN mRNA levels on day 1 ($P \leq 0.05$) and resulted in a further rise on day 2 ($P \leq 0.001$). IL-13 similarly led to a significant increase in POSTN mRNA on day 2 ($P \leq 0.01$). In HNFs, both IL-4 and IL-13 induced significant upregulation of POSTN mRNA on day 2 ($P \leq 0.001$) (Fig. 2C).

To compare overall periostin production between the two cell types, equal numbers of HNECs and HNFs were seeded and periostin concentrations in their culture media were quantified following IL-4 treatment. At both day 1 and day 2, HNFs secreted significantly higher levels of periostin than HNECs under equivalent cell numbers ($P \leq 0.001$) (Fig. 2D).

These findings indicate that periostin production in the nasal mucosa is differentially regulated by Th2 cytokines in epithelial cells and fibroblasts. While IL-4 is the primary inducer in HNECs, both IL-4 and IL-13 are effective regulators in HNFs. Moreover, HNFs are the dominant source of periostin, and its secretion increases progressively over time. These results support a model in which periostin is a key mediator of Th2-driven sinonasal inflammation, with distinct regulatory mechanisms operating in epithelial and mesenchymal cell populations.

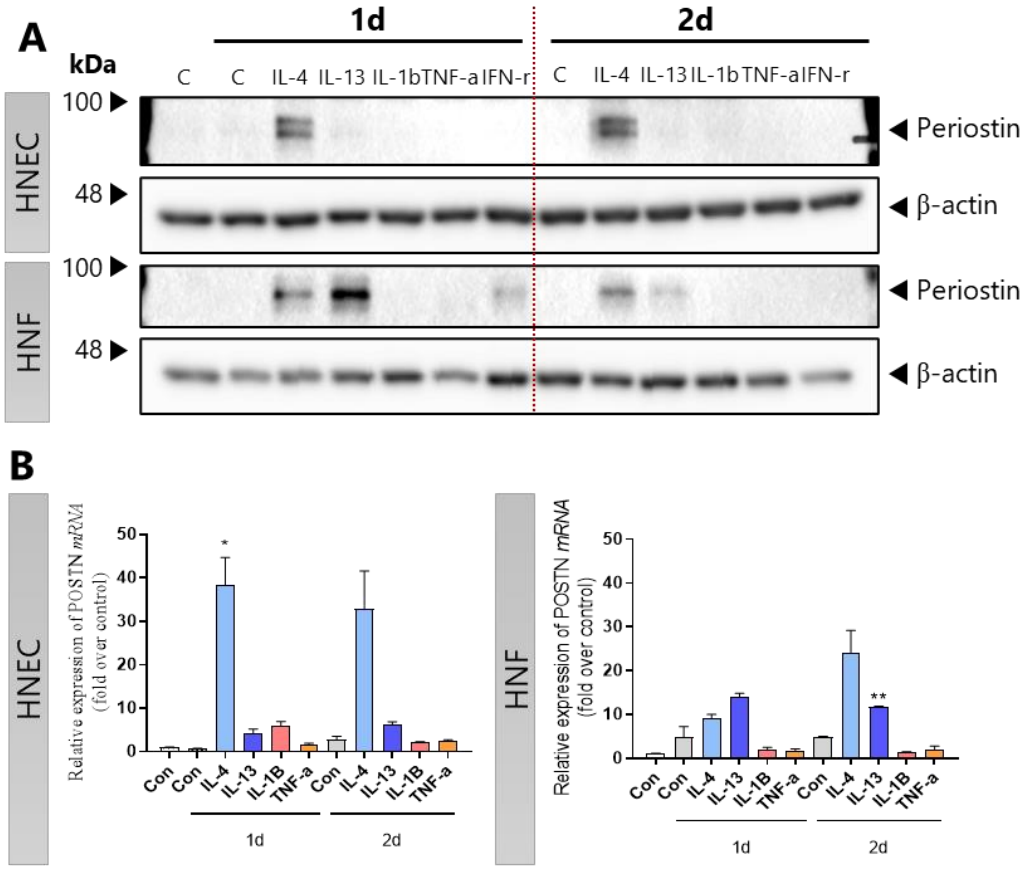

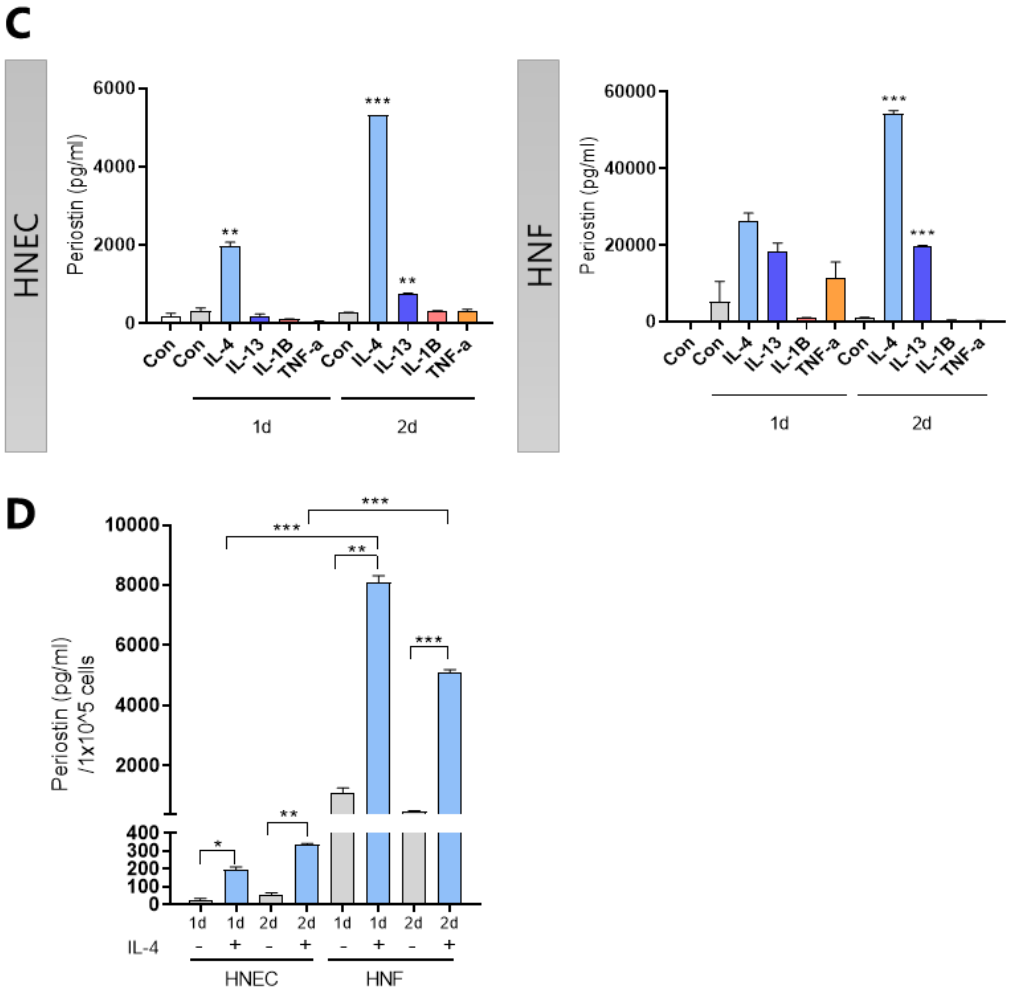

Figure 2. Periostin expression in human nasal cells by cytokines . HNEC and HNF cultured from human nasal polyp. Each cytokines treated same concentration(5ng/ml) (A) Comparison of expression levels of periostin between cytokines stimulated HNEC and HNF from Days 0 to 2. b-actin serves as a loading control. (B) Quantitative RT-PCR for POSTN in mRNA samples from HNEC and HNF treated with or without cytokines. (C) Level of periostin in concentration media of HNEC and HNF by ELISA. (D) Comparative analysis of periostin secretion per equivalent number of cells quantified by ELISA. *P ≤ 0.05, **P ≤ 0.01, ***P ≤ 0.001, vs control.

3.3. Periostin increased by co-culture of HNEC and HNF

To investigate the interaction between periostin produced by human nasal epithelial cells (HNECs) and human nasal fibroblasts (HNFs), a co-culture experiment was performed in the presence of IL-4, a cytokine known to elevate periostin levels in nasal cells. The aim was to determine whether these two cell types could mutually influence periostin production in a shared environment. A non-contact co-culture system was established using Transwell inserts, with HNECs cultured at the air–liquid interface (ALI) on the upper insert and HNFs cultured in the bottom well of the plate. HNECs were differentiated at ALI for 14 days to better simulate the in vivo nasal epithelial environment (Fig. 3A).

First, periostin protein levels in the cell lysates of both HNECs and HNFs were analyzed. In the co-culture condition, periostin expression was increased in both cell types compared to monoculture, with a more pronounced effect observed in HNFs. These results suggest that bidirectional signaling between epithelial cells and fibroblasts enhances periostin production, particularly in fibroblasts (Fig. 3B).

Next, mRNA expression of POSTN, the gene encoding periostin, was measured. In HNECs, co-culture with HNFs led to a significant increase in POSTN mRNA levels on day 1 ($P \leq 0.05$), indicating that fibroblasts stimulate periostin gene expression in epithelial cells (Fig. 3C). In contrast, HNFs showed a trend toward increased POSTN mRNA expression on day 1 in co-culture, but this change was not statistically significant, suggesting that periostin production in HNFs may be regulated predominantly at the post-transcriptional or protein level.

To assess the polarity of periostin secretion in epithelial cells, the apical side of HNECs was washed with PBS and periostin levels were measured by ELISA. No detectable periostin was found in the apical wash, indicating that periostin is secreted primarily toward the basolateral compartment (Fig. 3D).

Furthermore, analysis of the basolateral media revealed that periostin secretion was significantly higher in the co-culture group than in the combined media of separately cultured cells, particularly after IL-4 stimulation. At both day 1 ($P \leq 0.01$) and day 2 ($P \leq 0.001$), co-cultured cells secreted significantly greater amounts of periostin, indicating a synergistic effect on secretion in response to Th2 inflammation (Fig. 3E).

Collectively, these findings demonstrate that interactions between HNECs and HNFs synergistically enhance periostin production and secretion in response to IL-4. The non-contact co-

culture system highlights the importance of epithelial–mesenchymal crosstalk in the sinonasal microenvironment and further suggests that communication between fibroblasts and epithelial cells amplifies periostin-driven responses during Th2 inflammation.

A

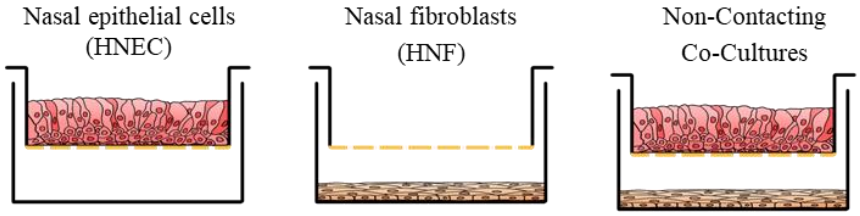

B

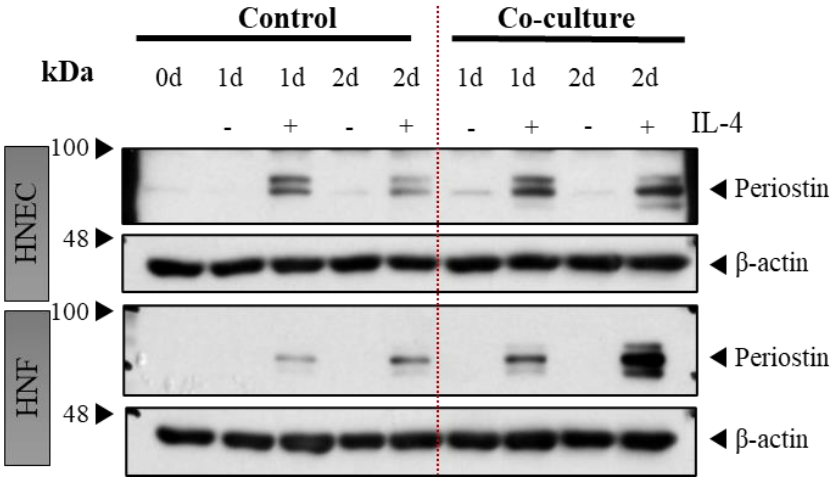

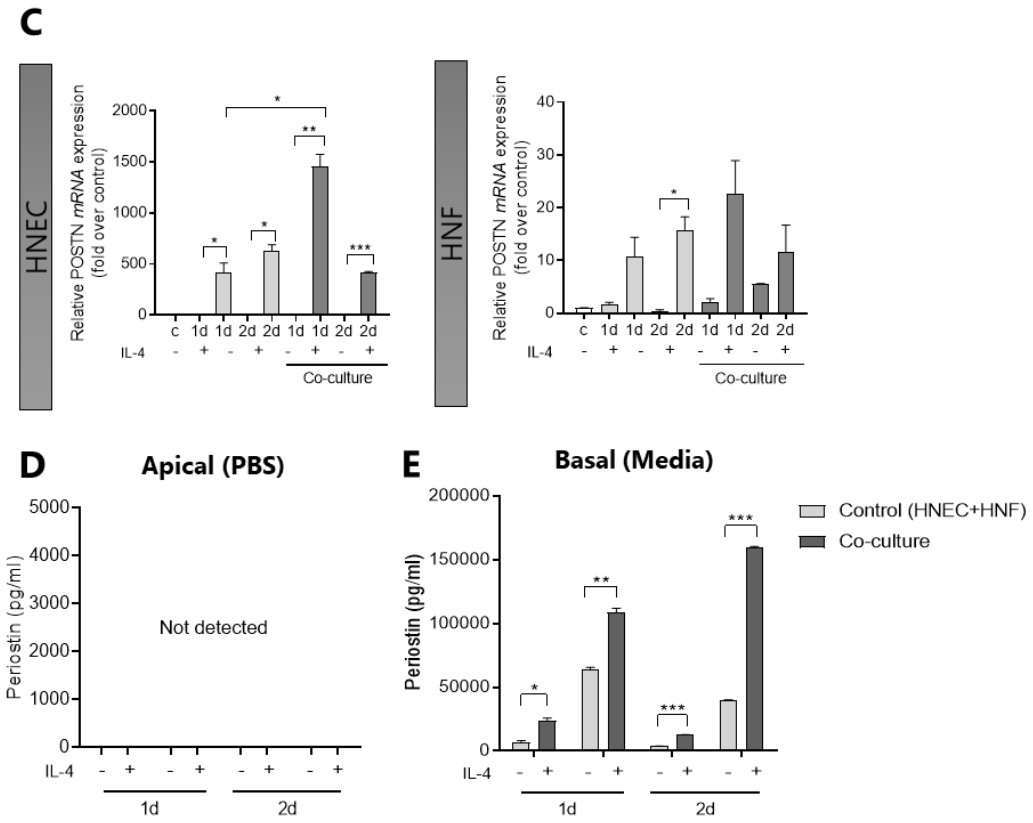

Figure 3. Level of periostin from co-culture of HNEC and HNF with IL-4. (A)Non-contacting co-culture with human nasal epithelial cells and fibroblasts (B)Comparison of expression level of periostin between separated culture and non-contacting co- culture of HNEC and HNF from Days 0 to 2. b-actin serves as a loading control. (C) Quantitative RT-PCR for POSTN in mRNA samples from HNEC and HNF each culture method. (D) Level of periostin in PBS which wash apical of HNEC analyzed by ELISA. (E) Level of periostin in concentration media of HNEC, HNF and co-culture analyzed by ELISA. *P ≤ 0.05, **P ≤ 0.01, ***P ≤ 0.001, **** P ≤ 0.0001, vs control.

3.4. Secreted periostin from nasal fibroblast mediates osteogenesis of MG63

MG63 osteoblast-like cells were employed to investigate the impact of periostin secreted from human nasal fibroblasts (HNFs) on osteogenic differentiation. The osteogenic differentiation of MG63 cells was induced for 10 days using osteogenic induction medium. To assess the role of fibroblast-derived periostin, conditioned media were collected from IL-4-treated HNFs, concentrated, and referred to as Secretion (HNF). The periostin concentration in Secretion (HNF) was quantified by ELISA and adjusted to match the level of recombinant human periostin for comparative analysis.

To determine whether the observed effects were dependent on periostin, a periostin-neutralizing antibody was added to Secretion (HNF) prior to MG63 treatment. After 10 days of differentiation, the number of alkaline phosphatase (ALP)-positive cells was significantly increased in the Secretion(HNF) group compared to both the control and Secretion (HNF) + antibody groups ($P \leq 0.01$), indicating enhanced osteogenic activity that was suppressed by periostin neutralization (Fig. 4A, B).

In addition, the mRNA expression levels of ALP and osteocalcin (OCN), which are key markers of osteogenic differentiation, were analyzed by qPCR. ALP mRNA levels were significantly elevated in the Secretion (HNF) group relative to the control and antibody-treated groups ($P \leq 0.01$), and OCN mRNA levels were even more profoundly upregulated ($P \leq 0.001$). These transcriptional changes paralleled the ALP staining results, and periostin-neutralized Secretion(HNF) significantly reduced the expression of both markers (Fig. 4C).

Collectively, these results indicate that periostin secreted by IL-4-treated nasal fibroblasts is essential for promoting the osteogenic differentiation of MG63 cells. The enhancement of osteogenic activity and marker gene expression was abrogated by periostin neutralization, confirming that fibroblast-derived periostin directly promotes osteogenesis in the setting of Th2-type inflammation.

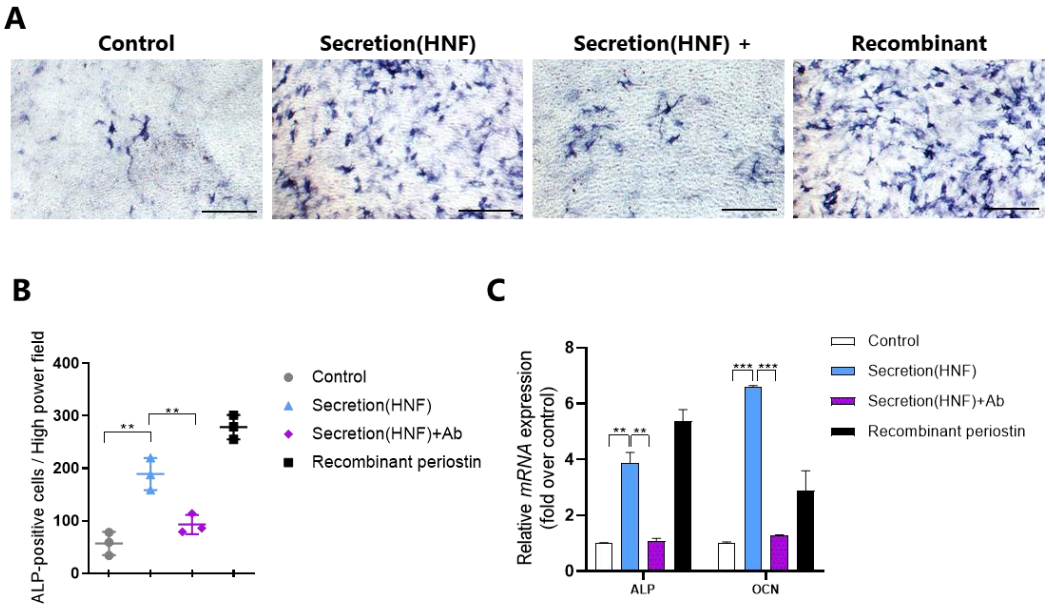

Figure 4. Secreted periostin from nasal fibroblasts by IL-4 mediated osteogenesis of MG63. (A) Comparison of differentiated osteoblast-like cell (MG63) by ALP staining . MG63 treated for 10 days with secretion from HNF, recombinant periostin and periostin blocking antibody. Scale bar = 500um. (B) The numbers of ALP-positive cells were counted in high-power field. (C) Quantitative RT-PCR for osteogenesis marker (ALP, Osteonectin) in mRNA samples from MG63. *P $\leq$ 0.05, **P $\leq$ 0.01, ***P $\leq$ 0.001.

3.5. Effect of periostin deficiency in the ECRS mouse model

3.5.1. Expression of periostin in nasal mucosa of the ECRS mouse model

To confirm the role of periostin in inflammatory diseases, periostin knockout (KO) mice were used and compared with wild-type (WT) controls. Based on data from human CRS patients, the eosinophilic CRS (ECRS) murine model was selected as an appropriate system for studying inflammation. ECRS groups were treated intranasally with a mixture of house dust mite (HDM), *Aspergillus fumigatus*, *Alternaria alternata*, and protease from *Staphylococcus aureus* three times per week for 12 weeks (Fig. 5). This allergen cocktail induces Th2 inflammation in the nasal cavity and recapitulates ECRS features such as goblet cell hyperplasia, polyp-like lesions, and peripheral blood eosinophilia.

First, periostin expression in the nasal mucosa was detected and compared in the WT groups. In particular, the WT ECRS group exhibited significantly higher levels of periostin in tissue lysates than controls, consistent with findings from ECRS patients. As expected, periostin protein was not detected in any KO group (Fig. 6A). At the mRNA level, POSTN was highly expressed in the WT ECRS group compared to the WT PBS group, while both KO groups showed negligible expression, confirming efficient gene knockout (Fig. 6B).

IHC further supported these results by revealing periostin expression localized to the subepithelial region of the nasal mucosa in WT mice. Expression was most pronounced in the ventral meatus of the nasal cavity, with the WT ECRS group showing higher periostin expression than the WT PBS group. In contrast, the KO groups had no detectable periostin expression, in agreement with the protein and qPCR data (Fig. 6C).

These findings demonstrate that periostin is upregulated in the nasal mucosa under ECRS conditions in wild-type mice. The absence of periostin expression in knockout mice confirms both the specificity of the gene ablation and the essential role of periostin in the pathophysiology of ECRS.

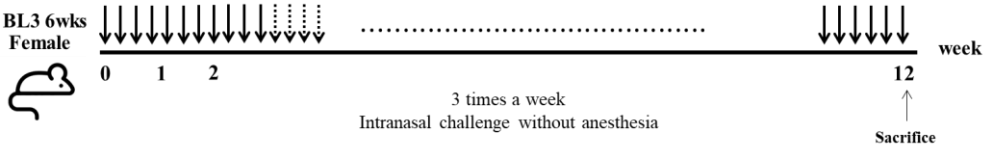

Group	Geno	
1	WT	**PBS**
2	WT	**ECRS**
3	Periostin ko	**PBS**
4	Periostin ko	**ECRS**

Group 1,3 (n=4) **: PBS (30μl)**

Group 2,4 (n=4) : **Alternaria (20μg) + Aspergillus (20μg) + HDM (Dp) (20μg) + Protease from *S. aureus* (1μg) in 30μl PBS**

Figure 5. Protocols for the development of eosinophilic rhinosinusitis in WT and periostin knock-out mice. Phosphate-buffered saline (PBS) was used for control groups (1 and 3). Alternaria, Aspergillus, HDM and Protease from Staphylococcus aureus diluted in PBS(30ul) was used as a intranasal challenge 3 times weeks in ECRS groups(2 and 4).

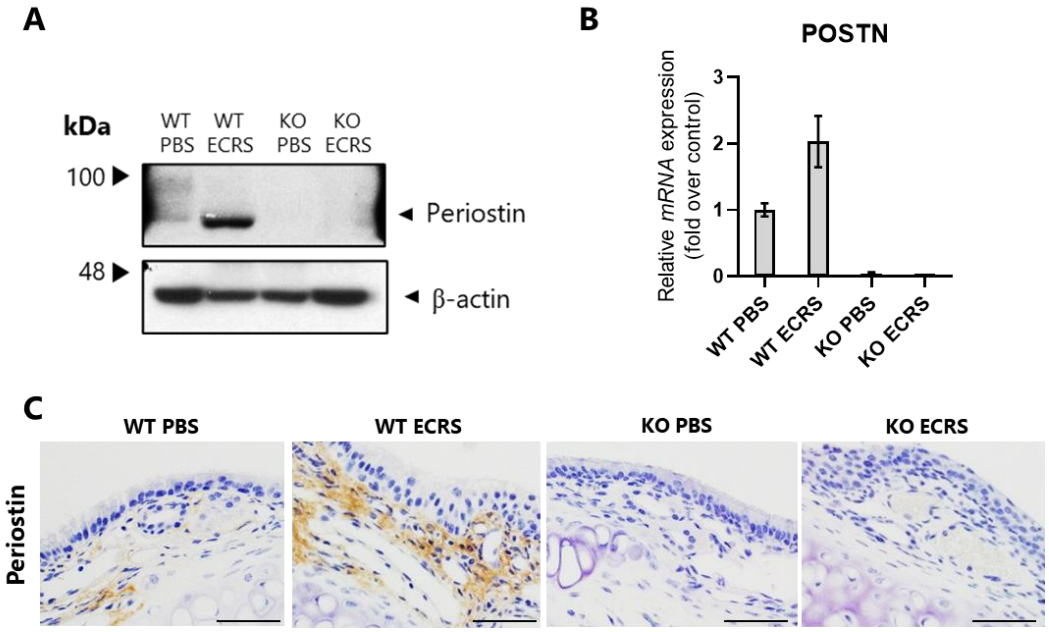

Figure 6. Periostin expression in the nasal mucosa of WT and periostin KO mice in the ECRS model. (A) Comparison of expression level of periostin from nasal mucosa between groups. (B) Quantitative RT-PCR for POSTN in mRNA samples from nasal mucosa of groups (C) Representative photomicrographs of immucochemistry (original magnification: × 400) showing periostin expression in the groups (scale bar: 50 μm).

3.5.2. Effects of periostin deficiency on inflammation in the ECRS mouse model

Next, I evaluated eosinophil infiltration in the nasal mucosa, which is an essential pathological feature of ECRS, using Sirius Red staining. The staining results demonstrated that both ECRS groups (WT ECRS and KO ECRS) exhibited substantial eosinophil infiltration in the nasal mucosa. In contrast, mice in the WT PBS and KO PBS groups showed no eosinophil infiltration, indicating a baseline absence of this inflammatory response under non-ECRS conditions (Fig. 7A).

Quantitative analysis confirmed that the numbers of infiltrating eosinophils were significantly higher in the WT ECRS group than in the WT PBS group ($P \leq 0.001$), and in the KO ECRS group than in the KO PBS group ($P \leq 0.01$). This increase was consistently observed across multiple anatomical sites of the nasal cavity, including the ventral meatus (WT: $P \leq 0.05$; KO: $P \leq 0.01$), nasal septum (WT: $P \leq 0.01$; KO: $P \leq 0.05$), and maxillary turbinate (WT and KO: $P \leq 0.001$). Notably, the number of eosinophils in the maxillary turbinate was significantly higher in the WT ECRS group compared to the KO ECRS group ($P \leq 0.05$) (Fig. 7B).

Despite the lack of periostin expression in the KO groups, the degree of eosinophil infiltration in KO ECRS mice was largely comparable to that observed in the WT ECRS group. This finding suggests that periostin is not required for the localization or infiltration of eosinophils in the nasal mucosa under ECRS conditions. These results indicate that periostin is not a critical determinant of eosinophil recruitment and infiltration into the nasal mucosal tissue.

I then utilized Periodic Acid-Schiff (PAS) staining to assess goblet cell hyperplasia in the nasal mucosa. Goblet cells, which play a pivotal role in mucus secretion, were evaluated to understand their response under ECRS conditions. The analysis demonstrated a significant increase in goblet cell numbers in both WT ECRS and KO ECRS groups compared to their respective PBS controls ($P \leq 0.05$ for both comparisons) (Fig. 8A). This hyperplasia reflects enhanced mucus production associated with ECRS in the nasal mucosa.

Notably, goblet cells were more frequently observed in the nasal septum than in the maxillary turbinate, suggesting a region-specific response in goblet cell proliferation. Despite the overall increase, goblet cell numbers in the ventral meatus were slightly lower in KO ECRS mice than in KO PBS controls ($P \leq 0.05$), whereas in the maxillary turbinate, goblet cells were significantly more abundant in WT ECRS mice than in WT PBS mice ($P \leq 0.05$) (Fig. 8B). Although these results show that ECRS induces goblet cell hyperplasia, there were no significant differences

between the WT ECRS and KO ECRS groups. This suggests that the absence of periostin does not impact the extent of goblet cell proliferation in the context of ECRS. The findings from PAS staining corroborate the results obtained from other assessments, indicating that while periostin plays a role in the pathology of ECRS, it is not essential for the proliferation of goblet cells in the nasal mucosa.

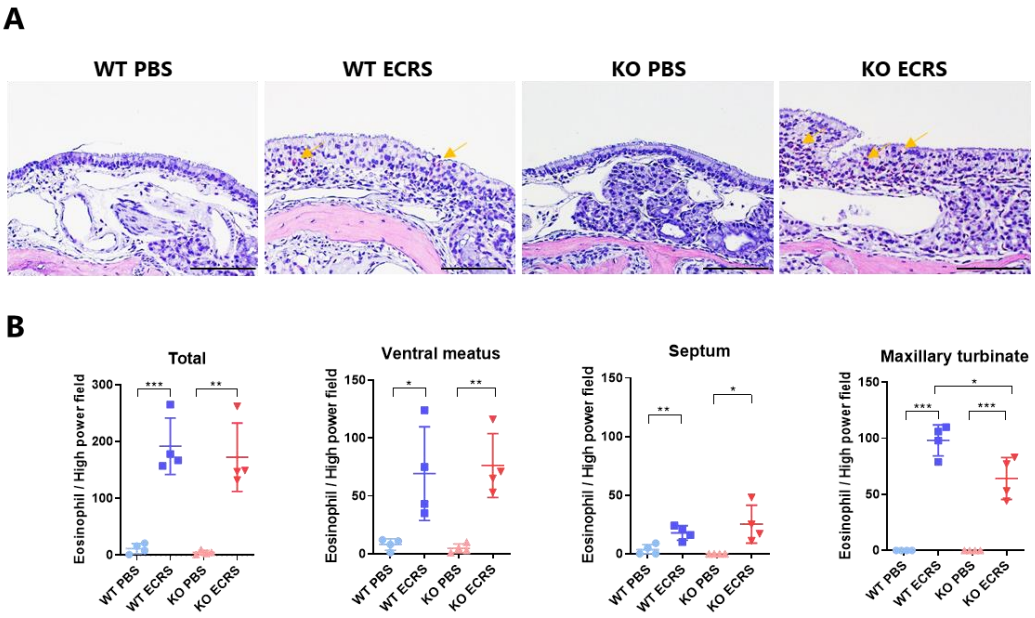

Figure 7. Effect of periostin deficiency on eosinophil infiltration in the ECRS mouse model. (A) Representative photomicrographs of Sirius red stain showing eosinophil infiltration in the group (scale bar: 50 μm). (B) The numbers of eosinophil were counted at septum, maxillary turbinate and ventral meatus in nasal cavity. *P ≤ 0.05, **P ≤ 0.01, ***P ≤ 0.001.

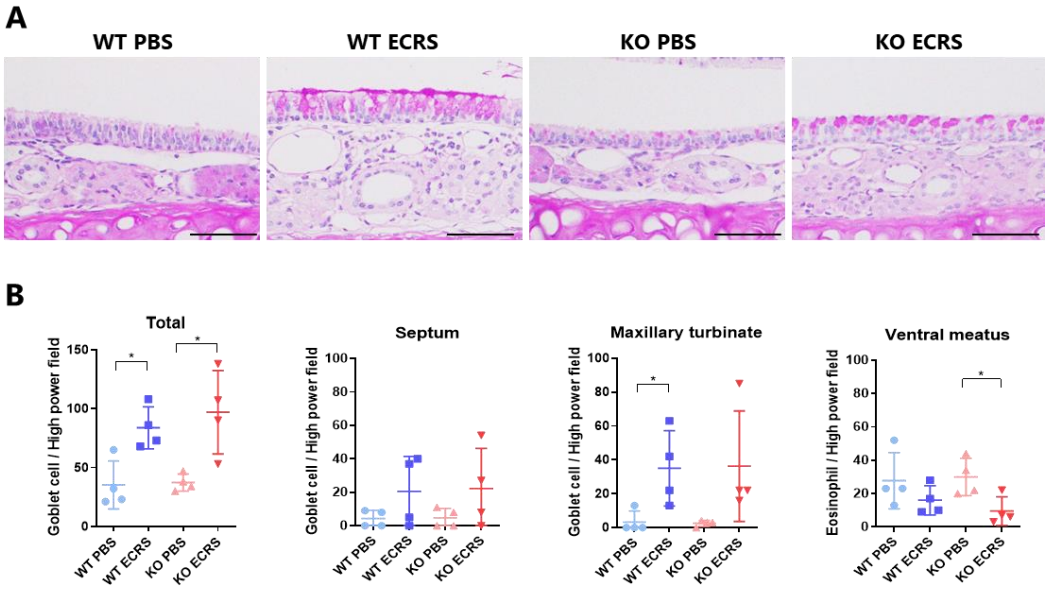

Figure 8. Effect of periostin deficiency on goblet cell hyperplasia in the ECRS mouse model. (A) Representative photomicrographs of periodic acid–Schiff stain showing goblet cell hyperplasia in the groups (scale bar: 50 μm). (B) The numbers of goblet cells were counted at septum, maxillary turbinate and ventral meatus in nasal cavity.*P ≤ 0.05.

3.5.3. Effects of periostin deficiency on osteitic changes in the ECRS mouse model

Moreover, IHC demonstrated the presence of RUNX2-positive cells along the perimeter of the nasal bone, especially in areas adjacent to the subepithelium (Fig. 9A). RUNX2 is a key transcription factor that regulates osteogenic activity, and its detection indicates active bone formation. The number of RUNX2-positive cells was significantly greater in the WT ECRS group than in the WT PBS group ($P \leq 0.001$), suggesting that ECRS conditions promote osteogenesis. In contrast, the KO ECRS group showed no significant difference in RUNX2-positive cell counts compared to the KO PBS group, and had significantly fewer RUNX2-positive cells than the WT ECRS group ($P \leq 0.01$) (Fig. 9B). These findings indicate that periostin is essential for RUNX2-mediated osteogenesis in the nasal mucosa.

Further supporting these results, measurements of bone thickness in the ventral meatus revealed that the nasal bone was significantly thicker in the WT ECRS group compared to the WT PBS group ($P \leq 0.05$) and the KO ECRS group ($P \leq 0.01$) (Fig. 9C). This enhanced bone thickening in WT ECRS mice suggests a periostin-dependent increase in osteogenesis under ECRS conditions.

Additionally, IF staining revealed strong expression of osteopontin, a marker of osteitis, along the nasal bone edge. Osteopontin immunoreactivity colocalized with periostin expression, implying a potential functional interaction or co-regulation between these proteins (Fig. 9D). Osteopontin levels in the nasal mucosa were significantly increased only in the WT ECRS group; there was no significant difference between the KO PBS and KO ECRS groups (Fig. 9E). These findings support the conclusion that periostin is critical for osteopontin expression and for the osteogenic and osteitic responses during ECRS. The absence of periostin in knockout mice prevented the upregulation of these osteogenic markers, resulting in reduced bone thickening and inflammation. Collectively, these results highlight the central role of periostin in ECRS-associated bone remodeling.

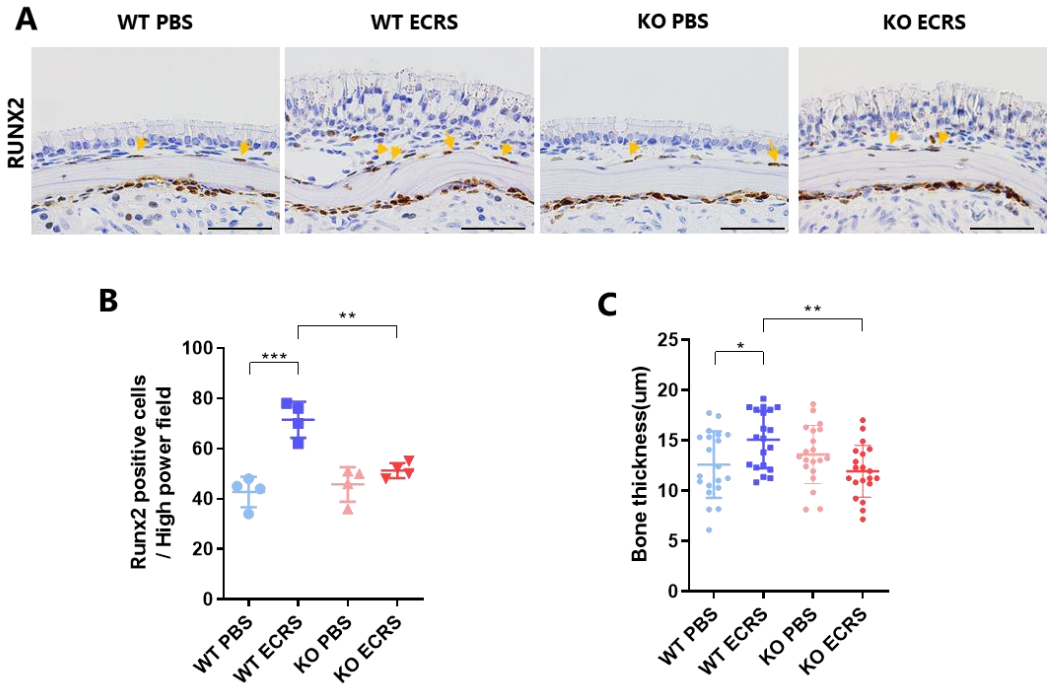

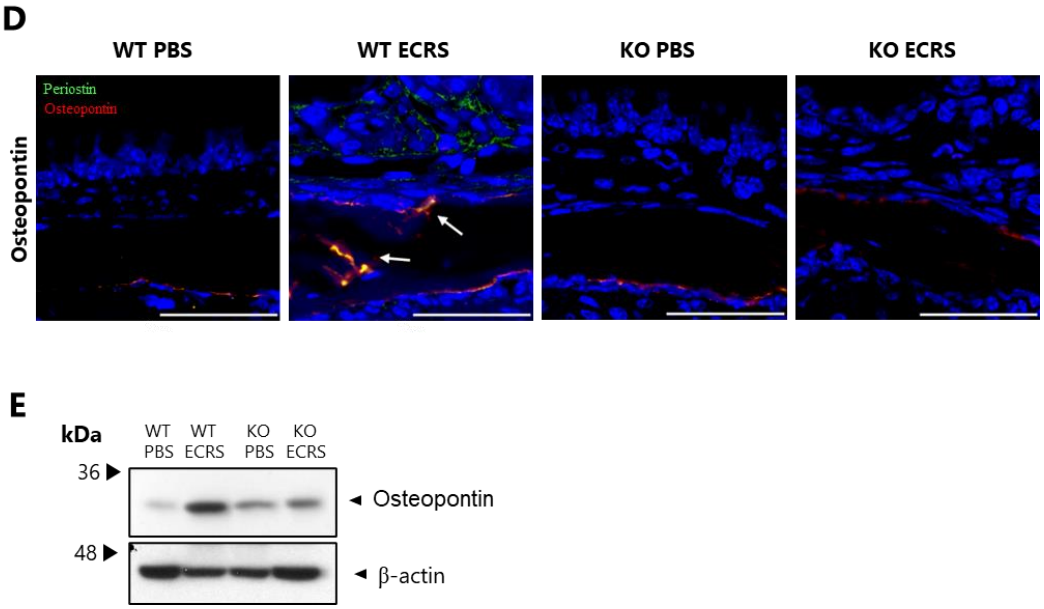

Figure 9. Effect of periostin deficiency on osteogenesis in the ECRS mouse model. (A) Representative photomicrographs of immucochemistry for RUNX2 from ventral meatus area in nasal cavity(scale bar: 50 μm). (B) The numbers of RUNX2 positive cells were counted at subepithelium side of nasal bone. (C) Bone thickness measured ventral meatus area in nasal cavity. (D) Representative immunofluorescence images of periositn (green), Osteopontin (Red), and nuclei (DAPI) from ventral meatus area in nasal cavity(scale bar: 50 μm). Arrowpoint show colocalization of perisotin and osteopontin(Yellow). (E) Comparison of expression level of osteopontin in nasal mucosa between groups. b-actin serves as a loading control. *P ≤ 0.05, **P ≤ 0.01, ***P ≤ 0.001.

3.5.4. Effects of periostin deficiency on tissue remodeling in the ECRS mouse model

Masson's trichrome staining was used to visualize collagen in the subepithelial region of the nasal mucosa. Collagen fibers appeared blue, which allowed clear distinction between the epithelial and subepithelial layers, and maximal thickness of each layer was measured at three points per region. The results indicated that both epithelial and subepithelial thicknesses were significantly increased in the ECRS groups compared to their respective PBS controls. In the ventral meatus, epithelial thickness was significantly greater in the WT ECRS group than in the WT PBS group ($P \leq 0.001$), and in the KO ECRS group than in the KO PBS group ($P \leq 0.001$). KO ECRS mice also showed further increases in epithelial thickness compared to WT ECRS mice ($P \leq 0.05$). In the nasal septum, both WT and KO ECRS groups displayed significantly increased epithelial thickness relative to their PBS controls ($P \leq 0.001$). In the maxillary turbinate, epithelial thickness was significantly elevated in WT ECRS ($P \leq 0.01$) and KO ECRS mice ($P \leq 0.001$) (Fig. 10B).

For the subepithelial region, the KO ECRS group exhibited greater thickness than the KO PBS group in the ventral meatus ($P \leq 0.01$), and was also significantly thicker than the WT ECRS group ($P \leq 0.05$). In the septum, subepithelial thickness was greater in the WT ECRS group than in the KO ECRS group ($P \leq 0.05$).

To quantify fibrosis, collagen deposition in the subepithelium was measured as the percentage of blue-stained area using Adobe Photoshop. Both ECRS groups showed significantly increased collagen-positive area compared to their PBS counterparts ($P \leq 0.05$), indicating fibrotic remodeling under chronic inflammatory conditions. However, there was no significant difference between WT ECRS and KO ECRS mice in collagen content (Fig. 10C).

Epithelial collapse was observed in both ECRS groups (Fig. 10D). Quantification revealed that KO ECRS mice had a significantly greater frequency of collapse regions compared to WT ECRS mice ($P \leq 0.05$), suggesting that periostin deficiency increases epithelial structural instability during chronic inflammation (Fig. 10E).

To further explore extracellular matrix (ECM) remodeling, immunofluorescence staining was performed for α-SMA and fibronectin. Eosinophils were identified by EMBP (white), which was used to evaluate possible colocalization with periostin (green). Such colocalization was not observed, but EMBP was localized to the subepithelium in both ECRS groups.

Both α-SMA and fibronectin (red) were specifically upregulated in WT ECRS mice. Fibronectin also colocalized with periostin in fibroblasts exhibiting a stellate morphology (Fig. 10F).

Western blot analysis further confirmed ECM remodeling. While α-SMA expression showed no significant differences among groups, fibronectin expression was increased in WT ECRS mice, consistent with immunofluorescence results (Fig. 10G).

These findings indicate that although periostin is not required for subepithelial collagen deposition, it plays a key role in regulating epithelial and subepithelial thickness and maintaining ECM integrity under inflammatory conditions. The prominent epithelial collapse observed in KO ECRS mice highlights the importance of periostin in preserving epithelial stability during chronic inflammation. Collectively, these results support that periostin may provide a protective function in sustaining nasal mucosal architecture in ECRS.

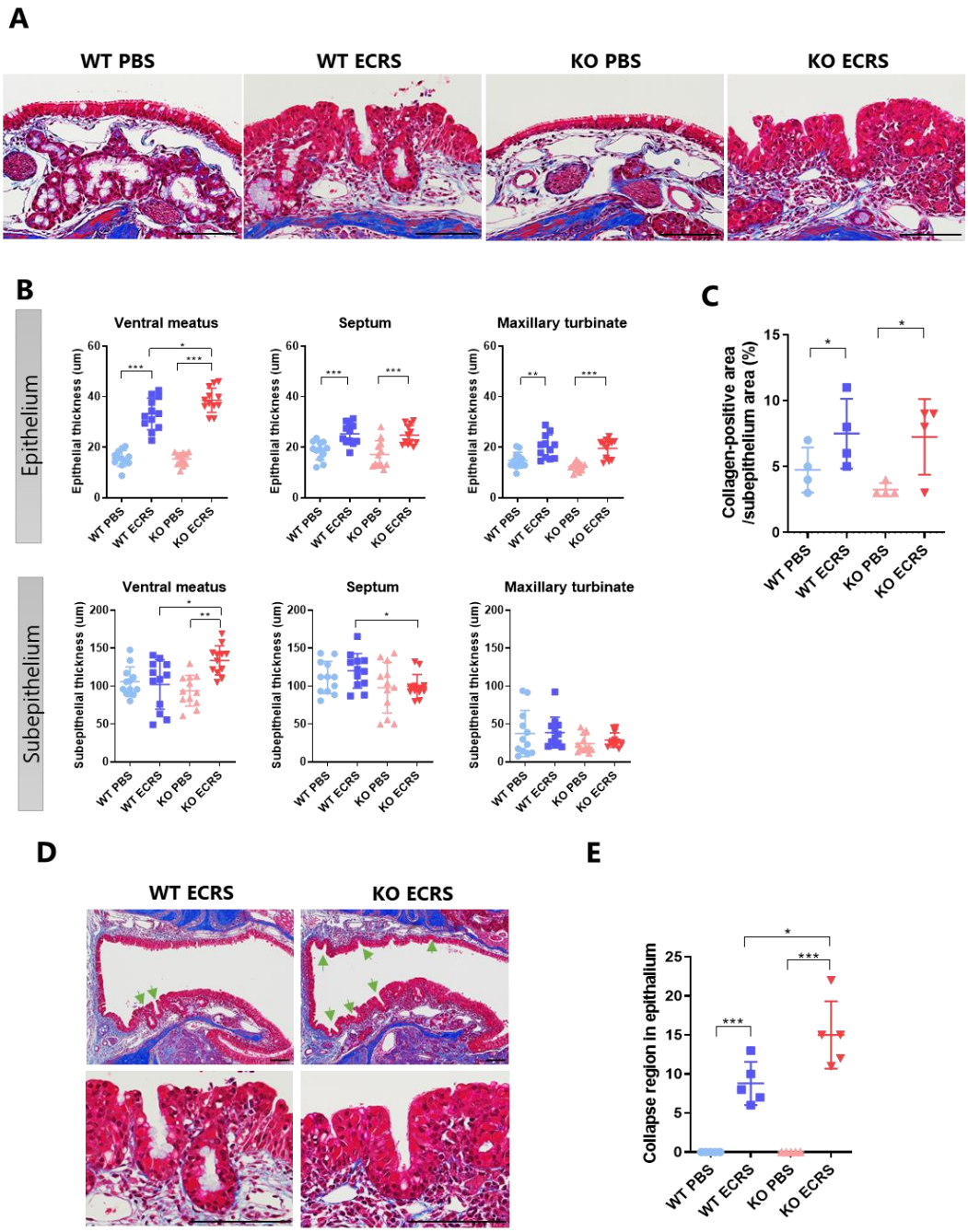

F

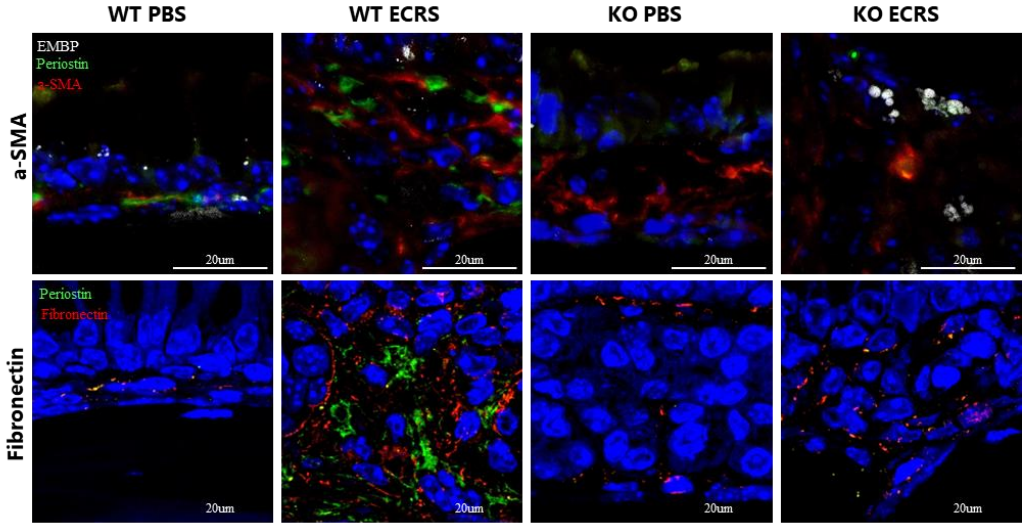

G

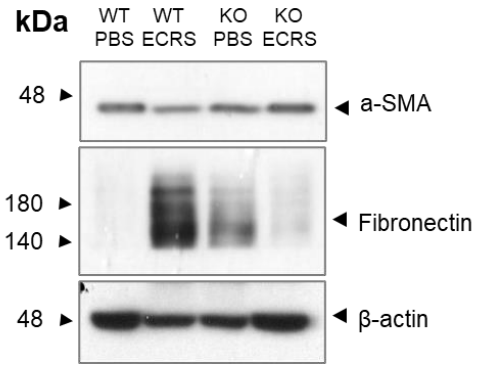

Figure 10. Effect of periostin deficiency on tissue remodeling in the ECRS mouse model. (A) Representative photomicrographs of Masson's trichrome stain showing collagen deposition in subepithelium of nasal mucosa in the groups (scale bar: 50 μm). (B) The thickness of epithelium were measured at septum, maxillary turbinate and ventral meatus in nasal cavity 3 times. (C) Percentage of collagen positive area in subepithelium in the groups. (D) Representative photomicrographs of epithelial collapse in WT and periostin ko ECRS group (scale bar: 50 μm). (E) The number of epithelial collapse were counted at nasal cavity. (F) Representative immunofluorescence images of periositn (green), a-SMA and fibronectin (Red), EMBP (White) and nuclei (DAPI) from ventral meatus area in nasal cavity(scale bar: 50 μm). (G) Comparison of expression level of a-SMA and fibronectin in nasal mucosa between groups. *$P \leq 0.05$, **$P \leq 0.01$, ***$P \leq 0.001$.

IV. DISCUSSION

Eosinophilic chronic rhinosinusitis with nasal polyps (ECRSwNP) patients have been reported to have higher levels of periostin and POSTN (mRNA) compared to non-ECRSwNP patients[42]. The results from the analysis of nasal ethmoid mucosa in CRS patients confirmed periostin expression differences between the ECRS group and the non-ECRS group, and demonstrated that the primary region of expression in the nasal mucosa is the subepithelium. This suggests an association between periostin and the pathophysiology of ECRS. Furthermore, measurements of sinonasal bone thickness revealed that both CRS groups had higher osteitis scores than the normal group. Moreover, the osteitis score in the ECRS group was significantly higher than in the non-ECRS group. The results showed that patients with ECRS had greater bone inflammation in the sinonasal area, indicating that periostin plays a significant role in osteogenic changes. This emphasizes the potential of periostin as an inducer of osteogenesis in CRS, as well as its connection to severe osteitis in ECRS.

Periostin is known to be upregulated by Th2 cytokines in multiple airway cells, such as fibroblasts, epithelial cells, and endothelial cells[7-11,43,44]. The results from human nasal cells stimulated with various cytokines confirmed periostin inducers in each nasal cell type. The level of periostin in cell lysates and POSTN (the gene encoding periostin) was induced by IL-4 in human nasal epithelial cells (HNECs), and by IL-4 and IL-13 in human nasal fibroblasts (HNFs). Also, secreted periostin in media was increased by the same cytokines in each cell type. Moreover, HNFs secreted more periostin under IL-4 stimulation than under IL-13, and the level of periostin induced by IL-4 increased over time. This differential response to interleukins may be attributable to differences in receptor types on HNFs and HNECs. When cell numbers were equalized, periostin concentrations in the media were higher from HNFs than from HNECs. This indicates that HNFs are the main source of periostin under Th2 cytokine stimulation, and that periostin expression increases over time in a chronic Th2 inflammatory environment as seen in ECRS.

A non-contact co-culture setup was used, with HNECs maintained under air-liquid interface (ALI) conditions and HNFs plated on the bottom of the well, in order to mimic the nasal epithelium environment and examine the interactions affecting periostin secretion between HNECs and HNFs. The results show that periostin levels in cell lysates increased in both HNECs and HNFs when co-cultured, suggesting that their interaction leads to higher periostin induction. Co-culture significantly increased POSTN mRNA levels in HNECs on day 1, indicating that the presence of HNFs

upregulates periostin gene expression in epithelial cells. However, no significant difference in POSTN mRNA levels was detected in HNFs between co-culture and separate culture, suggesting that periostin production in HNFs may be regulated more at the protein level. Additionally, periostin was detected only in the basolateral media of HNECs, indicating that periostin from HNECs is primarily secreted toward the basal side. Media from the co-culture group showed greater secretion than the combined media of the separately cultured groups, indicating that HNECs and HNFs have a synergistic effect in enhancing periostin synthesis under Th2 inflammation.

To investigate the role of secreted periostin in osteogenesis, conditioned media from HNFs treated with IL-4 was applied to MG63 cells, a human osteoblast-like cell line. Compared to control media, both the recombinant periostin group and the secretion (HNF) group exhibited significant increases in alkaline phosphatase (ALP)-positive cells, indicating enhanced osteogenic activity. When periostin in the secretion was neutralized using an antibody, osteogenic activity was significantly reduced. Similarly, ALP and osteocalcin (OCN) mRNA levels were significantly elevated in the secretion (HNF) and recombinant periostin groups but suppressed in the periostin-neutralized group. These findings confirm that secreted periostin directly contributes to osteogenic differentiation.

In vivo studies using ECRS murine models confirmed periostin expression in the nasal mucosa of WT groups, with WT ECRS showing higher levels of both protein and mRNA, while KO groups lacked periostin expression. Periostin localization was primarily observed in the subepithelium and was more pronounced in WT ECRS than in WT PBS, indicating that periostin expression is upregulated by ECRS-related inflammation.

Eosinophil infiltration, a hallmark of ECRS, was observed in both WT and KO ECRS groups, but not in PBS groups. No significant differences in eosinophil numbers were found between KO PBS and KO ECRS, suggesting that periostin is not essential for eosinophil recruitment. Similarly, goblet cell hyperplasia was significantly increased in both ECRS groups compared to PBS controls, with no difference between WT and KO ECRS groups, indicating that periostin is not required for this feature either.

RUNX2-positive cells, indicative of osteogenesis, were increased in WT ECRS but not in KO ECRS. Bone thickness was also higher in WT ECRS. Immunofluorescence showed periostin colocalized with osteopontin in nasal bone, with elevated levels observed only in WT ECRS. These results suggest that periostin promotes osteogenesis by activating RUNX2 and inducing osteopontin in ECRS.

In addition, epithelial and subepithelial thickening were observed in both ECRS groups, but KO ECRS showed more pronounced thickening and epithelial collapse than WT ECRS. Collagen deposition in the subepithelium increased in both groups without significant difference. These findings suggest that periostin may have a protective role in maintaining epithelial structure during chronic inflammation, possibly by preventing aberrant tissue remodeling.

These findings are consistent with prior studies showing that periostin expression persists at elevated levels in ECRS and may serve as a biomarker for endotyping and disease prognosis[45]. Its subepithelial localization and association with osteitis severity support a role in bone remodeling and osteogenesis in CRS[32]. Previous studies have described the involvement of periostin in tissue remodeling and suggested its relevance as a therapeutic target in type 2 inflammatory airway diseases, although some of these studies were conducted in the context of allergic conjunctivitis[46].

Additionally, the identification of nasal fibroblasts as a major source of periostin following Th2 cytokine stimulation aligns with clinical and experimental observations implicating fibroblasts in periostin-mediated tissue alterations. However, it should be noted that some supporting findings derive from studies in idiopathic pulmonary fibrosis[47] and atopic dermatitis[48], and thus may require cautious interpretation when applied to ECRS. The cooperative interaction between epithelial cells and fibroblasts in the context of Th2 cytokine stimulation contributes to the chronic inflammatory microenvironment characteristic of ECRS, a mechanism that has also been observed in other Th2-dominant conditions where periostin enhances epithelial cell activation and survival[48].

Additionally, the identification of nasal fibroblasts as a major source of periostin following Th2 cytokine stimulation aligns with clinical and experimental observations implicating fibroblasts in periostin-mediated tissue alterations in ECRS. The cooperative interaction between epithelial cells and fibroblasts under Th2 cytokine stimulation contributes to the chronic inflammatory microenvironment characteristic of ECRS.

Periostin functions as a key modulator of both pathological and reparative mechanisms in ECRS by facilitating osteogenic activity while contributing to epithelial structure maintenance. A lack of periostin has been shown to impair epithelial barrier integrity and reduce markers of osteogenesis, reflecting its multifaceted role in both disease development and mucosal preservation. Interventions that modulate periostin levels may offer potential approaches to regulate bone remodeling processes while supporting epithelial homeostasis in ECRS.

While these results advance understanding of periostin involvement in ECRS, several limitations remain. Most mechanistic insights are derived from murine models, which may not fully replicate human pathophysiology, particularly with respect to chronic immune interactions. Small sample sizes in human studies limit generalizability, and the use of immortalized cell lines may not accurately reflect the behavior of primary cells. Additionally, this study did not comprehensively explore interactions between periostin and other extracellular matrix components or cytokines.

Future research should validate these findings in larger and more diverse patient populations, utilize primary human cells for functional assays, and explore periostin isoforms and their regulatory mechanisms. Clinical trials are warranted to assess the efficacy and safety of periostin-targeted therapies in ECRS. Additionally, integrating periostin with other biomarkers could improve diagnostic and prognostic accuracy.

Overall, periostin is critical for proper nasal mucosa remodeling and maintenance and plays a significant role in osteogenesis under inflammatory conditions. Its multifaceted roles suggest that periostin could be a potential therapeutic target for managing chronic inflammation and tissue remodeling in ECRS (Figure.11).

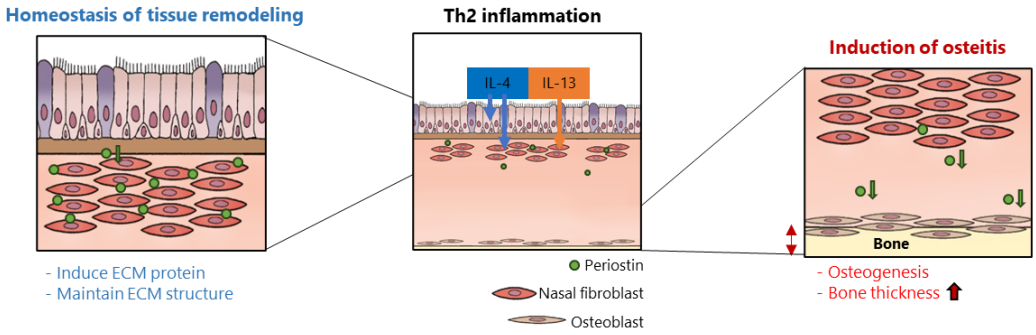

Figure 11. The two faces of periostin in ECRS. Perisotin induced by Th2 cytokines in nasal epithelium. In chronic inflammation, secreted perisotin help maintain ECM structure during tissue repair damaged by inflammation and induce osteitis in nasal bone activating osteoblast maturation.

V. CONCLUSION

In the context of Th2 inflammation, periostin expression is upregulated by IL-4 in human nasal epithelial cells (HNECs) and by both IL-4 and IL-13 in human nasal fibroblasts (HNFs). HNFs are the primary source of periostin, and their co-culture with HNECs synergistically enhances periostin secretion, indicating active crosstalk between these cell types.

In osteoblast-like MG63 cells, periostin secreted from IL-4-stimulated nasal fibroblasts enhances osteogenic differentiation, as demonstrated by increased alkaline phosphatase (ALP) activity and osteocalcin expression. These findings indicate that periostin functions as a key mediator linking Th2-type inflammation to pathological bone remodeling in the sinonasal mucosa, potentially contributing to osteitis through aberrant osteogenesis.

Although periostin is known to interact with eosinophils in other allergic diseases, its deficiency did not reduce eosinophil infiltration in the ECRS murine model, suggesting that periostin is not essential for eosinophil recruitment in this context.

Importantly, periostin plays a protective role in maintaining epithelial structure and extracellular matrix (ECM) integrity during chronic inflammation. Periostin-deficient mice exhibited increased epithelial collapse and reduced fibronectin expression, despite no significant changes in α-SMA or collagen levels. This indicates that periostin supports structural homeostasis, likely through its interaction with fibronectin, rather than general fibrotic remodeling.

In summary, periostin acts as both a mediator of inflammatory bone remodeling and a protector of epithelial and ECM integrity in eosinophilic chronic rhinosinusitis (ECRS), suggesting its potential as a novel therapeutic target for this chronic inflammatory disease.

References

1. Takeshita S, Kikuno R, Tezuka K, Amann E. Osteoblast-specific factor 2: cloning of a putative bone adhesion protein with homology with the insect protein fasciclin I. Biochemical Journal 1993;294:271-8.
2. Litvin J, Zhu S, Norris R, Markwald R. Periostin family of proteins: Therapeutic targets for heart disease. The Anatomical Record Part A: Discoveries in Molecular, Cellular, and Evolutionary Biology 2005;287A:1205-12.
3. Ruan K, Bao S, Ouyang G. The multifaceted role of periostin in tumorigenesis. Cellular and Molecular Life Sciences 2009;66:2219-30.
4. Xu D, Xu H, Ren Y, Liu C, Wang X, Zhang H, et al. Cancer stem cell-related gene periostin: a novel prognostic marker for breast cancer. PLoS One 2012;7:e46670.
5. Corren J, Lemanske RF, Hanania NA, Korenblat PE, Parsey MV, Arron JR, et al. Lebrikizumab treatment in adults with asthma. N Engl J Med 2011;365:1088-98.
6. Naik PK, Bozyk PD, Bentley JK, Popova AP, Birch CM, Wilke CA, et al. Periostin promotes fibrosis and predicts progression in patients with idiopathic pulmonary fibrosis. Am J Physiol Lung Cell Mol Physiol 2012;303:L1046-56.
7. Inai K, Norris RA, Hoffman S, Markwald RR, Sugi Y. BMP-2 induces cell migration and periostin expression during atrioventricular valvulogenesis. Developmental Biology 2008;315:383-96.
8. Conway SJ, Izuhara K, Kudo Y, Litvin J, Markwald R, Ouyang G, et al. The role of periostin in tissue remodeling across health and disease. Cellular and Molecular Life Sciences 2014;71:1279-88.
9. Hwang EY, Jeong MS, Park E-K, Kim JH, Jang SB. Structural characterization and interaction of periostin and bone morphogenetic protein for regulation of collagen cross-linking. Biochemical and Biophysical Research Communications 2014;449:425-31.
10. Seshadri S, Lu X, Purkey MR, Homma T, Choi AW, Carter R, et al. Increased expression of the epithelial anion transporter pendrin/SLC26A4 in nasal polyps of patients with chronic rhinosinusitis. Journal of Allergy and Clinical Immunology 2015;136:1548-58.e7.
11. Wang M, Wang X, Zhang N, Wang H, Li Y, Fan E, et al. Association of periostin expression

with eosinophilic inflammation in nasal polyps. Journal of Allergy and Clinical Immunology 2015;136:1700-3.e9.

12. Hoersch S, Andrade-Navarro MA. Periostin shows increased evolutionary plasticity in its alternatively spliced region. BMC Evolutionary Biology 2010;10:30.
13. Kii I, Ito H. Periostin and its interacting proteins in the construction of extracellular architectures. Cell Mol Life Sci 2017;74:4269-77.
14. Nakama T, Yoshida S, Ishikawa K, Kobayashi Y, Abe T, Kiyonari H, et al. Different roles played by periostin splice variants in retinal neovascularization. Exp Eye Res 2016;153:133-40.
15. Horiuchi K, Amizuka N, Takeshita S, Takamatsu H, Katsuura M, Ozawa H, et al. Identification and characterization of a novel protein, periostin, with restricted expression to periosteum and periodontal ligament and increased expression by transforming growth factor beta. J Bone Miner Res 1999;14:1239-49.
16. Sonnenberg-Riethmacher E, Miehe M, Riethmacher D. Promotion of periostin expression contributes to the migration of Schwann cells. J Cell Sci 2015;128:3345-55.
17. Litvin J, Selim AH, Montgomery MO, Lehmann K, Rico MC, Devlin H, et al. Expression and function of periostin-isoforms in bone. J Cell Biochem 2004;92:1044-61.
18. Morra L, Rechsteiner M, Casagrande S, von Teichman A, Schraml P, Moch H, et al. Characterization of periostin isoform pattern in non-small cell lung cancer. Lung Cancer 2012;76:183-90.
19. Bai Y, Nakamura M, Zhou G, Li Y, Liu Z, Ozaki T, et al. Novel isoforms of periostin expressed in the human thyroid. Jpn Clin Med 2010;1:13-20.
20. Kim CJ, Isono T, Tambe Y, Chano T, Okabe H, Okada Y, et al. Role of alternative splicing of periostin in human bladder carcinogenesis. Int J Oncol 2008;32:161-9.
21. Norris RA, Damon B, Mironov V, Kasyanov V, Ramamurthi A, Moreno-Rodriguez R, et al. Periostin regulates collagen fibrillogenesis and the biomechanical properties of connective tissues. J Cell Biochem 2007;101:695-711.
22. Oka T, Xu J, Kaiser RA, Melendez J, Hambleton M, Sargent MA, et al. Genetic manipulation of periostin expression reveals a role in cardiac hypertrophy and ventricular remodeling. Circ Res 2007;101:313-21.
23. Kudo A, Kii I. Periostin function in communication with extracellular matrices. J Cell

Commun Signal 2018;12:301-8.

24. Xu M, Chen D, Zhou H, Zhang W, Xu J, Chen L. The Role of Periostin in the Occurrence and Progression of Eosinophilic Chronic Sinusitis with Nasal Polyps. Sci Rep 2017;7:9479.
25. Uchida M, Shiraishi H, Ohta S, Arima K, Taniguchi K, Suzuki S, et al. Periostin, a matricellular protein, plays a role in the induction of chemokines in pulmonary fibrosis. Am J Respir Cell Mol Biol 2012;46:677-86.
26. Norris RA, Moreno-Rodriguez R, Hoffman S, Markwald RR. The many facets of the matricelluar protein periostin during cardiac development, remodeling, and pathophysiology. J Cell Commun Signal 2009;3:275-86.
27. Conway SJ, Izuhara K, Kudo Y, Litvin J, Markwald R, Ouyang G, et al. The role of periostin in tissue remodeling across health and disease. Cell Mol Life Sci 2014;71:1279-88.
28. Blanchard C, Mingler MK, McBride M, Putnam PE, Collins MH, Chang G, et al. Periostin facilitates eosinophil tissue infiltration in allergic lung and esophageal responses. Mucosal Immunology 2008;1:289-96.
29. Gordon ED, Sidhu SS, Wang Z-E, Woodruff PG, Yuan S, Solon MC, et al. A protective role for periostin and TGF-β in IgE-mediated allergy and airway hyperresponsiveness. Clinical & Experimental Allergy 2012;42:144-55.
30. Rosenfeld RM, Andes D, Bhattacharyya N, Cheung D, Eisenberg S, Ganiats TG, et al. Clinical practice guideline: Adult sinusitis. Otolaryngology - Head and Neck Surgery 2007;137:S1-S31.
31. Fujieda S, Imoto Y, Kato Y, Ninomiya T, Tokunaga T, Tsutsumiuchi T, et al. Eosinophilic chronic rhinosinusitis. Allergol Int 2019;68:403-12.
32. Stankovic KM, Goldsztein H, Reh DD, Platt MP, Metson R. Gene expression profiling of nasal polyps associated with chronic sinusitis and aspirin-sensitive asthma. Laryngoscope 2008;118:881-9.
33. Ninomiya T, Noguchi E, Haruna T, Hasegawa M, Yoshida T, Yamashita Y, et al. Periostin as a novel biomarker for postoperative recurrence of chronic rhinosinitis with nasal polyps. Scientific Reports 2018;8:11450.
34. Jia G, Erickson RW, Choy DF, Mosesova S, Wu LC, Solberg OD, et al. Periostin is a systemic biomarker of eosinophilic airway inflammation in asthmatic patients. Journal of

Allergy and Clinical Immunology 2012;130:647-54.e10.

35. Kanemitsu Y, Matsumoto H, Mishima M. Factors Contributing to an Accelerated Decline in Pulmonary Function in Asthma. Allergology International 2014;63:181-8.
36. Johansson MW, Annis DS, Mosher DF. α(M)β(2) integrin-mediated adhesion and motility of IL-5-stimulated eosinophils on periostin. Am J Respir Cell Mol Biol 2013;48:503-10.
37. Shiono O, Sakuma Y, Komatsu M, Hirama M, Yamashita Y, Ishitoya J, et al. Differential expression of periostin in the nasal polyp may represent distinct histological features of chronic rhinosinusitis. Auris Nasus Larynx 2015;42:123-7.
38. Bhandarkar ND, Sautter NB, Kennedy DW, Smith TL. Osteitis in chronic rhinosinusitis: a review of the literature. Int Forum Allergy Rhinol 2013;3:355-63.
39. Snidvongs K, McLachlan R, Chin D, Pratt E, Sacks R, Earls P, et al. Osteitic bone: a surrogate marker of eosinophilia in chronic rhinosinusitis. Rhinology 2012;50:299-305.
40. Zuo K, Guo J, Chen F, Xu R, Xu G, Shi J, et al. Clinical characteristics and surrogate markers of eosinophilic chronic rhinosinusitis in Southern China. European Archives of Oto-Rhino-Laryngology 2014;271:2461-8.
41. Park SC, Kim SI, Hwang CS, Cho H-J, Yoon J-H, Kim C-H. Multiple airborne allergen-induced eosinophilic chronic rhinosinusitis murine model. European Archives of Oto-Rhino-Laryngology 2019;276:2273-82.
42. Kim DW, Kulka M, Jo A, Eun KM, Arizmendi N, Tancowny BP, et al. Cross-talk between human mast cells and epithelial cells by IgE-mediated periostin production in eosinophilic nasal polyps. Journal of Allergy and Clinical Immunology 2017;139:1692-5.e6.
43. Asano M, Kubota S, Nakanishi T, Nishida T, Yamaai T, Yosimichi G, et al. Effect of connective tissue growth factor (CCN2/CTGF) on proliferation and differentiation of mouse periodontal ligament-derived cells. Cell Communication and Signaling 2005;3:11.
44. Norris RA, Potts JD, Yost MJ, Junor L, Brooks T, Tan H, et al. Periostin promotes a fibroblastic lineage pathway in atrioventricular valve progenitor cells. Developmental Dynamics 2009;238:1052-63.
45. Ebenezer JA, Christensen JM, Oliver BG, Oliver RA, Tjin G, Ho J, et al. Periostin as a marker of mucosal remodelling in chronic rhinosinusitis. Rhinology 2017;55:234-41.
46. Asada Y, Okano M, Ishida W, Iwamoto S, Fukuda K, Hirakata T, et al. Periostin deletion suppresses late-phase response in mouse experimental allergic conjunctivitis. Allergology

International 2019;68:233-9.

47. Murata K, Koga Y, Kasahara N, Hachisu Y, Nunomura S, Nakajima N, et al. Accumulation of periostin in acute exacerbation of familial idiopathic pulmonary fibrosis. J Thorac Dis 2018;10:E587-e91.

48. Shiraishi H, Masuoka M, Ohta S, Suzuki S, Arima K, Taniguchi K, et al. Periostin Contributes to the Pathogenesis of Atopic Dermatitis by Inducing TSLP Production from Keratinocytes. Allergology International 2012;61:563-72.

Abstract in Korean

부비동염 질환에서의 periostin의 역할

Periostin 은 천식, 만성 비부비동염 등 만성 호흡기 질환에서 제2형 염증의 바이오마커로 알려져 있으며, 조직의 재형성에 관여합니다. 만성 비부비동염 환자들에게서 조직과 혈청 내 periostin 이 증가한다는 보고들이 있었지만, 만성 비부비동염에서 정확히 어떤 역할을 하는지는 확립되지 않았습니다.

본 연구는 염증성 부비동염에서 periostin 의 주 분비 조직과 periostin 의 분비를 유도하는 사이토카인을 확인하고, 만성 염증으로 인해 증가하는 periostin 이 염증을 악화시키거나 조직 재형성으로부터 코 상피를 결론적으로 보호하는지, 분비된 periostin 이 골형성과의 연관성을 가지는지를 알아보고자 했습니다.

그 결과, 사람에게서 유래한 코 상피세포와 섬유아세포에 IL-4를 처리하였을 때, 두 세포의 세포 내 단백질, RNA, 배지에서 periostin 이 증가했습니다. Periostin 은 세포 수 대비 코 상피세포보다 코 섬유아세포에서 더 많이 분비되었으며, periostin 의 주요 공급원이 코 섬유아세포임을 확인했습니다. 또한, 코 섬유아세포에서 IL-4에 의해 분비된 periostin 은 조골세포의 분화를 유도합니다.

Periostin 유전자 제거(KO) 마우스를 이용하여 ECRS 마우스 모델에서 periostin 결핍에 의한 영향을 조사한 결과, 야생형 호산구 만성 부비동염(ECRS) 그룹은 비강 상피에서 periostin 발현이 증가하고 상피가 두꺼워졌으며, 비강 내 뼈 두께도 두꺼워진 것으로 나타났습니다. 또한 KO ECRS 는 WT ECRS 보다 코뼈에서 RUNX2 및 osteopontin 발현이 적었습니다. 그리고 세포외기질 단백질인 fibronectin 의 발현이 KO ECRS 에서 현저히 줄었습니다. 이에 따라 상피층은 비정상적인 형성으로 구조가 무너지는 양상을 보였습니다. 그러나 비강 상피의 호산구 침윤과 술잔세포의 증식에는 ECRS 군 간 차이가 유의하지 않았습니다.

Periostin 은 Th2 사이토카인에 의해 코 섬유아세포에서 주로 분비되며, 분비된 periostin 은 지속되는 조직 재형성에서 상피층 구조를 유지하는 데 관여하고, 비강 내 뼈의 골형성을 유도합니다. 결론적으로, 만성 부비동염에서 periostin 은 조직 구조 보호와 골형성 악화를 동시에 유도하는 양면성을 가집니다.

핵심되는 말 : periostin, 비강 점막, 골분화, 만성 비부비동염